# Onboard Hydrogen Generation for a Spark Ignition Engine via Thermochemical Recuperation

By

Isaac Alexander Silva
B.A. (UC Santa Cruz) 2008

Thesis

Submitted in partial satisfaction of the requirements for the degree of

Master of Science

in

Mechanical and Aerospace Engineering

in the

Office of Graduate Studies

of the

University of California

Davis

Approved:

---

Chair Dr. Paul Erickson, Chair

---

Dr. Joan Ogden

---

Dr. Benjamin Shaw

Committee in Charge

2014





ProQuest LLC.
789 East Eisenhower Parkway
P.O. Box 1346
Ann Arbor, MI 48106 - 1346

*To my fiancée, who never let me give up when times were tough ...*

*you are my inspiration*

# Contents

List of Figures . . . . . vi
List of Tables . . . . . viii
Abstract . . . . . ix
Acknowledgments . . . . . x

**1 Introduction** **1**
1.1 Motivation . . . . . 1
1.2 Background . . . . . 1
1.2.1 Internal combustion engines . . . . . 3
1.2.2 Hydrogen Production . . . . . 5
1.3 Problem Definition and Research Objectives . . . . . 6
1.3.1 Closed Loop Thermochemical Recuperation . . . . . 6

**2 Theory and Previous Research** **7**
2.1 Steam Reforming . . . . . 7
2.1.1 Fundamentals . . . . . 7
2.1.2 Conversion, Yield, and Efficiency . . . . . 8
2.1.3 Limiting Factors . . . . . 10
2.1.4 Catalyst Degradation . . . . . 14
2.1.5 Modeling . . . . . 17
2.2 Spark Ignition Engines . . . . . 17
2.2.1 Fundamentals . . . . . 17
2.2.2 Stoichiometry . . . . . 19
2.2.3 Exhaust Temperature . . . . . 20
2.2.4 Emissions . . . . . 20
2.2.5 Ignition Timing . . . . . 20
2.2.6 Hydrogen Assisted Combustion . . . . . 22
2.3 Thermochemical Recuperation . . . . . 25

2.3.1 Thermal Considerations . . . . . 26
2.3.2 Chemical Considerations . . . . . 26
2.3.3 Measures of Efficiency . . . . . 27
2.4 Contribution . . . . . 29

**3 Experimental Facility and Approach** **31**
3.1 Engine . . . . . 32
3.1.1 Ignition System . . . . . 32
3.1.2 Engine Stoichiometry . . . . . 32
3.1.3 Load Bank . . . . . 33
3.2 Steam Reformer . . . . . 34
3.2.1 Catalyst Bed . . . . . 35
3.2.2 Heat Exchanger . . . . . 37
3.3 Fuel Delivery System . . . . . 38
3.3.1 Water System . . . . . 39
3.3.2 Gas System . . . . . 40
3.3.3 Preheat System . . . . . 41
3.3.4 Control System . . . . . 41
3.3.5 Gas Analysis . . . . . 42
3.4 Experimental Procedure . . . . . 42
3.4.1 Start Up . . . . . 43
3.4.2 Operation . . . . . 44
3.4.3 Possible Faults and their detection . . . . . 46
3.5 Factorial Design . . . . . 48
3.5.1 Independent and Dependent Variables . . . . . 48
3.5.2 Randomization . . . . . 49
3.5.3 Statistical Analysis . . . . . 49

**4 Results and Discussion** **51**
4.1 Open Loop . . . . . 51

4.1.1 Engine Results . . . . . 51
4.1.2 Steam Reformer Results . . . . . 55
4.2 Closed Loop . . . . . 58
4.2.1 Efficiency . . . . . 58
4.2.2 Power . . . . . 61
4.2.3 Exhaust Temperature . . . . . 61
4.2.4 Stability Limit . . . . . 64
4.2.5 Exhaust Heat Recovery . . . . . 64
4.2.6 Other Characteristics . . . . . 66
4.2.7 Summary . . . . . 68

**5 Conclusions and Recommendations** **70**
5.1 Recommendations for Future Work . . . . . 70
5.1.1 Equipment Modifications . . . . . 70
5.1.2 Research Topics . . . . . 71

# List of Figures


1.1 World Energy Consumption . . . . . 2
1.2 Typical Energy Split in Gasoline Internal Combustion Engines . . . . . 4

2.1 Sooting Temperature Dependence . . . . . 16
2.2 Idealized Otto Cycle . . . . . 18
2.3 Emissions as a Function of fuel air equivalence ratio $\phi$ [1] . . . . . 21
2.4 Brake Thermal Efficiency vs. Equivalence ratio $\phi$ [2] . . . . . 23
2.5 Brake Specific $NO_x$ vs. Equivalence Ratio $\phi$ . . . . . 24
2.6 In Cylinder Pressure vs. Crank Angle for different Fuels [3] . . . . . 24
2.7 System Efficiency of a gasoline fueled engine with Thermochemical Recuperation . . . . . 29

3.1 Schematic of the Thermochemical Recuperation Experimental apparatus 31
3.2 Ignition System Schematic . . . . . 33
3.3 Load Bank Schematic . . . . . 34
3.4 Installed Steam Reformer . . . . . 35
3.5 Steam Reformer . . . . . 35
3.6 Steam Reformer Schematic . . . . . 36
3.7 Catalyst Pellets . . . . . 37
3.8 Fuel Delivery Schematic . . . . . 38
3.9 Water Flowmeter . . . . . 39
3.10 Mass Flow Controller . . . . . 40
3.11 Reformate Chiller Schematic . . . . . 42
3.12 Preheat Schematic (single heater) . . . . . 43
3.13 Control Schematic . . . . . 44
3.14 Exhaust line failure . . . . . 47
3.15 Coke buildup . . . . . 48

4.1 Open Loop Engine Brake Thermal Efficiency . . . . . 52

4.2 Power . . . . . 53
4.3 Exhaust Gas Temperature . . . . . 54
4.4 Conversion . . . . . 56
4.5 Yield . . . . . 57
4.6 Efficiency . . . . . 58
4.7 $\eta_{SYS}$ vs. % fuel stream reformed by volume . . . . . 59
4.8 $\eta_{SYS}$ vs. % $H_2$ in fuel stream . . . . . 59
4.9 Power vs. $\lambda$, % fuel stream reformed by volume . . . . . 62
4.10 Power vs. $\lambda$, % $H_2$ in fuel stream . . . . . 62
4.11 EGT vs. $\lambda$, % fuel stream reformed by volume . . . . . 63
4.12 EGT vs. $\lambda$, % $H_2$ by volume in fuel stream . . . . . 63
4.13 Tailpipe Exhaust Temperature $\mathrm{EGT}_{out}$ vs. Reactant Flow Rate and $\lambda$ . . 64
4.14 Heat Exchanger Efficiency vs. EGT & Reactant Flow Rate . . . . . 65
4.15 Heat Exchanger Loss vs. EGT & Reactant Flow Rate . . . . . 66
4.16 Percentage $H_2$ by volume in Fuel Stream . . . . . 67
4.17 Parasitic load vs. EGT & Reactant Flow Rate . . . . . 68

# List of Tables


3.1 Bosch LSU 4.9 Specifications . . . . . 32
3.2 Water Flowmeter Specifications . . . . . 39
3.3 Mass Flow Controllers . . . . . 41
3.4 Open Loop Engine Test Settings . . . . . 45
3.5 Open Loop Steam Reformer Test Settings . . . . . 46
3.6 Closed Loop Thermochemical Recuperation Test Settings . . . . . 46
3.7 Factors and corresponding levels . . . . . 48
3.8 Experimental design matrix . . . . . 49
3.9 Factorial Experiment Run Order . . . . . 49

4.1 Summary of factorial experiments . . . . . 60
4.2 Statistical analysis of factorial experiment results . . . . . 60
4.3 Effects and interactions of the input variables . . . . . 60
4.4 Signal-to-noise $t$-ratio and statistical significance . . . . . 61

# Abstract

**Onboard Hydrogen Generation for a Spark Ignition Engine via Thermochemical Recuperation**

A method of exhaust heat recovery from a spark-ignition internal combustion engine was explored, utilizing a steam reforming thermochemical reactor to produce a hydrogen-rich effluent, which was then consumed in the engine. The effects of hydrogen in the combustion process have been studied extensively, and it has been shown that an extension of the lean stability limit is possible through hydrogen enrichment. The system efficiency and the extension of the operational range of an internal combustion engine were explored through the use of a methane fueled naturally aspirated single cylinder engine co-fueled with syngas produced with an on board methane steam reformer. It was demonstrated that an extension of the lean stability limit is possible using this system.

# Acknowledgments

Many thanks to my professor, Dr. Paul Erickson, whose guidance and practical advice carried me through, and to my lab manager Dave Davieau, whose knowhow and experience kept me from most major pitfalls. To my mother and father, to whom I owe my interest in mechanical engineering, and who gave me encouragement to pursue my academic interests. To my lab mates at HyPAUL, who were a wonderful resource for my work. To my committee members, whose helpful advice and comments were indispensable.

# Nomenclature

| | |
|---|---|
| $\Delta\bar{h}_{RXN}$ | heat of reaction |
| $\Delta h_i$ | enthalpy change of process $i$ |
| $\dot{E}$ | generator power |
| $\dot{m}_i$ | mass flow rate of species $i$ |
| $\dot{Q}$ | heat flux |
| $\epsilon$ | catalyst bed void fraction |
| $\eta$ | efficiency |
| $\eta_{HX}$ | efficiency of heat exchanger |
| $\eta_{SR}$ | efficiency of steam reformer |
| $\eta_{sys}$ | efficiency of system |
| $\eta_{TH}$ | brake thermal efficiency |
| $\gamma$ | catalyst shape factor |
| $\gamma$ | ratio of specific heats |
| $\lambda$ | normalized air fuel equivalence ratio |
| $\nu$ | kinematic viscosity |
| $\phi$ | normalized fuel air equivalence ratio |
| $\rho$ | density |
| $\tau_{CK}$ | characteristic time of chemical kinetics |
| $\tau_{HT}$ | characteristic time of heat transfer |

$\tau_{MT}$ characteristic time of mass transfer

$\tilde{Y}_i$ yield of species $i$

$\varphi$ Thiele modulus

$ATR$ auto-thermal reactor

$C_p$ specific heat

$C_{AS}$ surface concentration

$COV_{imep}$ coefficient of variation in indicated mean effective pressure

$D$ diameter

$D$ diffusivity

$d$ diameter

$D_C$ combined Knudsen and external diffusivity

$d_{cat}$ catalyst diameter

$E_i$ effect of factor $i$

$I_{i,j}$ interaction of factors $i$ and $j$

$k$ reaction rate

$k_c$ mass transfer coefficient

$k_i$ rate coefficient for reaction $i$

$K_j$ adsorption constant for species $j$

$LHV_i$ lower heating value of species $i$

$Nu$ Nusselt number

$POX$ partial oxidation reactor

$Q$ heat

$q$ heat flux per unit area

$q'''$ heat generation per unit volume

$Q_{in}$ heat in

$Q_{loss}$ heat loss

$r$ compression ratio

$r_j$ formation rate of species $j$

$Re$ Reynold's number

$S/C$ steam to carbon ratio

$S_E$ standard error

$S_i^2$ variance of experimental configuration $i$

$S_p$ pooled standard deviation

$Sc$ Schmidt number

$Sh$ Sherwood number

$T_m$ mean temperature

$u$ fluid velocity

$X$ conversion

°BTDC degrees before top dead center

EGT exhaust gas temperature

MBT maximum brake torque

MFC mass flow controller

RPM revolutions per minute

TCR thermochemical recuperation

TDC top dead center

WOT wide open throttle

# Chapter 1

# Introduction

## 1.1 Motivation

Combustion engines and heat engines play a central role in our energy systems. In typical heat engine cycles there is a great deal of energy that is wasted and it is worthwhile to recover some of it. A large portion of this energy is in the form of thermal energy that is not extracted in the work cycle, as hot gases. In a large power plant or industrial setting this heat can be used as process heat either for other processes or further energy generation, but there are fewer options for smaller installations and mobile platforms. Several methods exist for the recovery of energy from these hot gases, including organic rankine cycle turbines, solid state thermoelectric devices, and thermochemical methods. Thermochemical methods may provide a straightforward way to recover energy for efficiency improvement.

## 1.2 Background

Since the industrial revolution changed forever our relationship to fire and energy, combustion systems have played a central part in our economic and technological development. From wood and coal fired steam engines to the modern power plants and sports cars, burning hydrocarbons dominates our power production. It is always advantageous to improve our use of our resources, and a great source of loss in combustion systems is heat rejection. There are limits to the efficiency of thermal systems based on thermodynamics,

however there is still significant room for improvement. Since its inception in the late 19th century, the internal combustion engine (*ICE*) has been a useful source of power. The ICE is relatively simple and power dense thus these engines changed the face of transportation by making cars practical and powered flight possible. As shown in Figure 1.1 worldwide energy has increased, and fossil fuels including oil and natural gas have fueled our modern age.

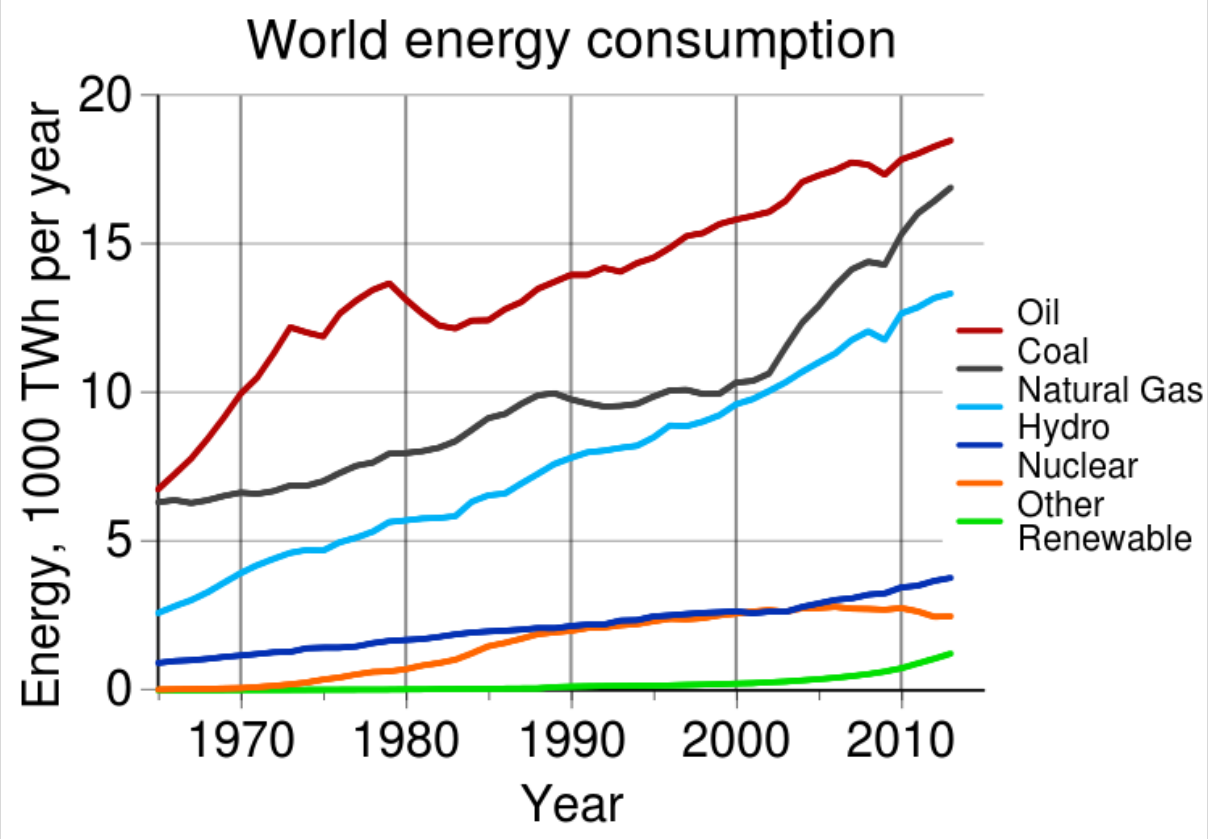


Figure 1.1: World energy consumption by type, 1965 - 2013

As our use of hydrocarbon fuels increased with our adoption of combustion engines, our knowledge about how to best use these fuels increased as well. Thick petroleum crude was refined into naphthalene, hexane, and octane, and we used catalytic processing plants to shape these hydrocarbons into the fuels that were desired. Central to this catalytic processing is hydrogen, which is used in varying amounts for all the fuels. Methods of producing hydrogen for use in the production of other fuels and chemicals were developed, among them steam reforming, in which a hydrocarbon fuel, typically methane, is injected

with water over a hot catalyst bed. The hydrogen is then separated from the resultant stream of $H_2$, $CO$, and $CO_2$. The heat for this endothermic reaction is usually from a portion of the feedstock being combusted.

### 1.2.1 Internal combustion engines

With the development of refined fuels, internal combustion engines could be developed. Thermodynamic cycles were described which these engines mimicked, including the otto cycle which represents a significant portion of all heat engines and is used widely in transportation. These engines had the advantage of being power dense, which made them attractive for automobiles and aircraft where weight is at a premium. As well they could run at a range of operating conditions which made them suitable for various drive cycles and environments.

#### 1.2.1.1 Hydrogen Enrichment

Hydrogen addition in internal combustion engines has been studied extensively, and shows some promise for improving efficiency due to a number of factors. Though the data are mixed, engines specifically designed for hydrogen usage have taken advantage of hydrogen's higher octane rating, high flame speed and wide flammability limit to make improvements in efficiency, emissions, and turndown ratios relative to comparable engines burning hydrocarbon fuels. Hydrogen enrichment has been shown to allow low pollutant emission operating points that were previously unattainable. Hydrogen fueled engines, and hydrogen enriched engines, have been shown to operate in much leaner conditions. Though often mistakenly heralded as an alternative fuel, as hydrogen does not exist by and large free in the environment it is best thought of as an energy carrier, as energy is required for its production. Some of the most prominent difficulties with hydrogen lie in its storage; it can be stored as a gas in compressed tanks, or as a liquid in cryogenic tanks, or even reversibly bonded to a metal hydride, but all these methods have poor energy density on a volumetric basis when compared with liquid fuels such as gasoline or ethanol, and have much more heavy and complex storage systems.

#### 1.2.1.2 Heat Recovery

Significant interest exists in heat recovery for combustion engines, as this represents the single largest loss in the system. As seen in Figure 1.2, the heat rejection accounts for as much as 70% of the combustion energy.

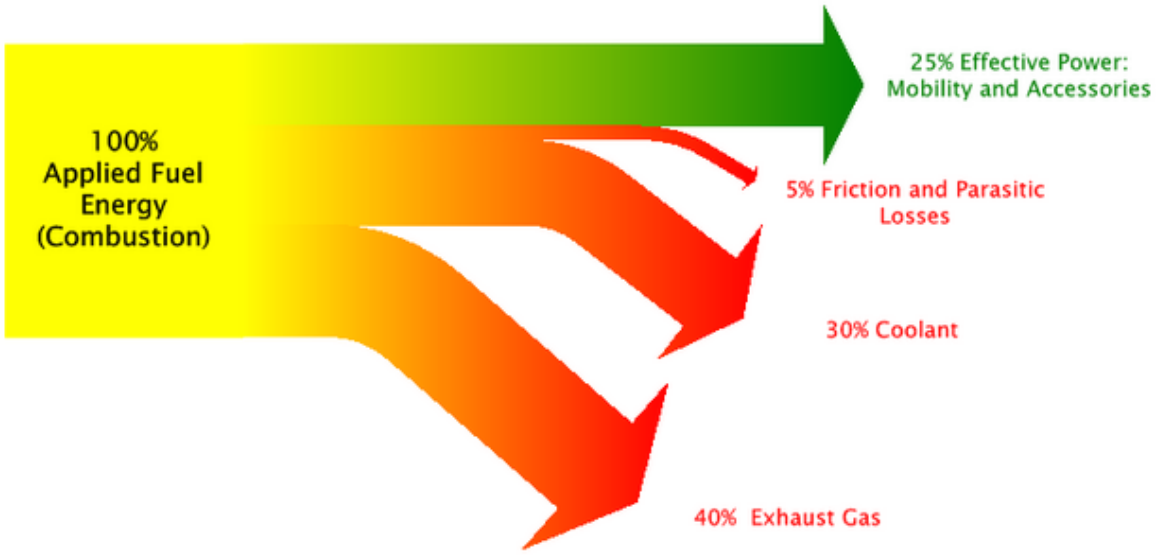


Figure 1.2: Typical Energy Split in Gasoline Internal Combustion Engines

Many methods of heat recovery have been developed, though primarily to boost power density rather than thermal efficiency. Some are in common usage, such as the turbocharger, while others such as solid state thermoelectric devices remain under research. Several chemical methods have been proposed, among them the production of hydrogen, both for combustion or for use in a fuel cell. Organic rankine cycles, which utilize a hydrocarbon based working fluid in a turbine, have also been researched as a method of heat recovery, and remain an ongoing interest for some systems [4–10].

Crucial to all heat recovery systems is the heat exchanger. Heat exchangers and heat exchanger design always plays a role - it is desirable to recover the maximum amount of heat, and many improvements in heat transfer come at the expense of pressure drop. Ideal heat exchanger design depends on the recovery method - thermoelectric generators have maximum operating temperatures and require a thermal gradient across the device, while for many thermochemical methods high temperatures and uniform bed temperatures are

desirable.

### 1.2.2 Hydrogen Production

Hydrogen is produced in a number of ways. A common way of producing hydrogen is through electrolysis. This is possible on a vehicle or in a plant, however industrially common methods of producing hydrogen are primarily thermochemical, and $H_2$ is produced through chemical decomposition of hydrocarbon fuels. There are three basic thermochemical methods, which are partial oxidation ($POX$), in which the fuel is catalytically combusted with insufficient air resulting in a $CO$ and $H_2$ rich effluent; steam reforming ($SR$), in which the fuel is reacted with water at elevated temperatures on a externally heated catalyst bed; and auto thermal reforming ($ATR$), in which the two processes are combined and the exothermic partial oxidation provides the heat for the endothermic steam reforming. Other methods of hydrogen production exist, such as thermolysis, in which water is heated to extreme temperatures to dissociate it; or other thermochemical cycles such as the sulfur iodine cycle; as well as biological pathways. Production is dominated, however, by steam reforming.

#### 1.2.2.1 Steam Reforming

Steam reforming is a highly endothermic process and is a significant portion of all hydrogen production activities. Steam reforming of methane is typically done in tubular reactors or reactor bundles, and operated at steady state for months or years at a time. Both because of the thermal mass of the catalyst and the endothermic nature of the reactions, this process has poor transient response relative to $POX$ or $ATR$. All energy used is provided externally, which make it useful for energy recovery. Other hydrocarbon fuels can be steam reformed, including propane and octane, as well as alcohols such as methanol and ethanol. Interest in the reforming of heavier hydrocarbons is primarily driven by the need to provide hydrogen for fuel cells and the generally poor energy storage properties of hydrogen.

## 1.3 Problem Definition and Research Objectives

Currently, there are few practical heat recovery devices on small scale plants and engines. It is desirable to extract the maximum amount of energy from a given fuel, so improved heat recovery should be considered. Thermochemical heat recovery presents an option to do this, through the generation of a higher energy content fuel. As well, the addition of hydrogen allows other operating conditions for the internal combustion engine including leaner operation and improved throttling; the inclusion of an onboard source of hydrogen from the primary feedstock allows the usage of hydrogen without a separate storage system. This project designed and built a small scale steam reformer heated by exhaust of a small internal combustion engine, ran the engine in part on the effluent of this reactor, and performed some preliminary performance investigations of the system.

### 1.3.1 Closed Loop Thermochemical Recuperation

The principle goal of this research is to examine the possibility of developing an onboard hydrogen generation method for the purposes of fuel enrichment, and to recover energy from the exhaust. To this end, multiple dimensions were explored:

- The design and construction of an effective heat exchanger to recover exhaust heat
- The design and construction of a chemical reactor capable of handling the expected flow rates, sized for the heat rate of the exhaust
- The development of a rudimentary control scheme, to control reactor conditions and monitor system performance
- Statistical analysis and model development based on acquired data

# Chapter 2

# Theory and Previous Research

## 2.1 Steam Reforming

Steam reforming is an endothermic process used to produce hydrogen from hydrocarbon feedstocks. Heat is added to the reactants of vaporized fuel and steam in a catalytic reactor. Typically in industrial settings this is performed over a nickel based catalyst in large pelletized catalyst beds. Some of the fuel feedstock is consumed to provide the heating, or the heat is provided from another process. The efficiency is dependent on reactor design, and is governed by three characteristics: heat transfer, mass transfer, and chemical kinetics. The effectiveness of the reactor is measured in several ways, depending on the system and the end use of the products; these included conversion, yield, and efficiency. As heat is applied externally to the reactor a temperature gradient from the inner wall of the reactor to the centerline is developed. Because the reaction rates are strongly temperature dependent every effort is made to reduce the temperature gradient to create more uniform conditions.

### 2.1.1 Fundamentals

The global steam reforming reaction for a general hydrocarbon fuel is

$$C_nH_m + SnH_2O \longrightarrow (\frac{m}{2} + 2n)H_2 + nCO_2 + (S-2)nH_2O \tag{2.1}$$

In Equation 2.1, $S$ is the steam to carbon ratio, and $n$ and $m$ are the number of carbon and hydrogen atoms, respectively. Steam to carbon ratios (S/C) can be predicted from a

global reaction balance, but this assumes that all reactions go to completion [11] and in practice S/C ratios are higher than the global balance to prevent coking. This additional steam is then condensed out of the product stream. Steam reforming is a complex process involving hundreds of reactions and many intermediate species. This has been explored by other researchers [12–14], however for the steam reforming of methane the process is dominated by three reactions. These are:

$$CH_4 + H_2O \longleftrightarrow CO + 3H_2 \qquad \Delta H_{298} = 2.06 \times 10^5 \ J/kmol \tag{2.2}$$

$$CO + H_2O \longleftrightarrow CO_2 + H_2 \qquad \Delta H_{298} = -4.10 \times 10^4 \ J/kmol \tag{2.3}$$

$$CH_4 + 2H_2O \longleftrightarrow CO_2 + 4H_2 \qquad \Delta H_{298} = 1.65 \times 10^5 \ J/kmol \tag{2.4}$$

Steam reforming can be considered to be governed by these reactions [13].The reaction rates in the steam reformer are a function of temperature, the fuel type, catalyst type and support, and concentration of species. All species approach equilibrium given sufficient time, and species concentrations can be shown to be a function of residence time. The maximum energy recovery in terms of the chemical potential of the fuel is not when the global reaction shown by Equation 2.1 goes to completion, but when there are significant amounts of $CO$ in the fuel stream. The importance of the composition of the reformate stream in terms of thermochemical recuperation are discussed below.

### 2.1.2 Conversion, Yield, and Efficiency

Conversion efficiency is one measure of reactor performance. It is defined as the difference between unity and the quotient of the molar flow rates out of and in to the reactor respectively of the reactant, as shown below in Equation 2.5.

$$X = 1 - \frac{(\dot{n}_{CH_4})_{outlet}}{(\dot{n}_{CH_4})_{inlet}} \tag{2.5}$$

Conversion is a very important metric as fuel decomposition represents most of the energy requirements of steam reforming. As steam reforming is endothermic, and heat is supplied externally, conversion is closely related to the heat transfer characteristics of the steam reformer[15].

Yield is the quotient of the molar flow rate of the desired product, in this case $H_2$, and the stoichiometric maximum possible available from the fuel in question.

$$\tilde{Y}_{H_2} = \frac{\dot{n}_{H_2}}{4\dot{n}_{CH_4}} \tag{2.6}$$

Equation 2.6 is a good measure of reactor performance when $H_2$ is desired, such as the case for hydrogen production for use in proton exchange membrane fuel cells, where high yields of $H_2$ and low yields for $CO$ are needed to prevent poisoning of the fuel cell. In this case however it may not be as useful as a measure of reactor performance, because the goal is to maximize the energy content of the reactor effluent, not to get a specific product. In this case, the endothermic reactions are what we are most interested in as they add usable chemical energy to our reformate stream, so Equation 2.5 is a more useful measure. Maximum energy recovery on a lower heating value basis occurs when reactions 2.2 and 2.4 dominate, and exothermic reaction 2.3 is minimized.

The efficiency of the steam reformer can be discussed in a number of ways [11]. A first definition considers the lower heating value ($LHV$), as shown below in Equation 2.7:

$$\eta_1 = \frac{LHV_{Product}}{LHV_{Reactant}} \tag{2.7}$$

in which $LHV_{Product}$ and $LHV_{Reactant}$ are the weighted average heating values of the product and reactant stream, respectively. This definition overlooks the heat input to the system, and can yield greater than 100% efficiency because of this omission. Arguably this is appropriate when evaluating the steam reformer as a component of a larger system in which the heat supplied is a byproduct of another process, and would otherwise be unrecovered. A more accurate definition which accounts for the added heat is shown below in Equation 2.8. This definition does not ignore the heat input and is a better system level approach:

$$\eta_2 = \frac{\dot{m}_{Product} LHV_{Product}}{\dot{m}_{Reactant} LHV_{Reactant} + Q_{in}} \tag{2.8}$$

Which definition is used is dependent on what the goals of analysis are.

### 2.1.3 Limiting Factors

One of the problems with comparing different reactor and catalyst geometries is that multiple parameters are linked, and cannot easily be separated. To compare different reactor designs pseudo non-dimentional parameters are used such as residence time, or its inverse, space velocity. Conventionally, space velocity is used as a non dimensional comparison, which is defined as shown in Equation 2.9,

$$GHSV = \frac{V_{CH_4}}{V_{catalyst\ bed}} \tag{2.9}$$

but this has been shown to be insufficient for comparing real reactors [16, 17]. A method that has proven successful is through the parameter characteristic time [17]. By modeling the reactor as a first order, plug flow reactor, the characteristic time can be inferred from measured conversion of the fuel, and different reactor geometries can be compared. Reactors with the same characteristic time have the same conversion of fuel at a given flow rate. The characteristic time includes all the information about the heat transfer, mass transfer, and chemical kinetics of the system, and is largely independent of mass flow rate provided the Reynolds number is sufficiently small [18]. The overall characteristic time can be considered to be the sum of the three limiting characteristic times of heat transfer, mass transfer, and chemical kinetics.

#### 2.1.3.1 Heat Transfer

The heat transfer can be described as the sum of two effects, heat input from the wall of the reactor and heat consumption from chemical reactions. From an energy balance, steam reforming in a tubular reactor can be described as

$$\frac{dT_m}{dx} = \frac{q''}{\rho C_p u}\frac{4}{D} - \frac{q'''}{\rho C_p u} \tag{2.10}$$

where $T_m$ is the mean temperature, $q''$ is the heat flux from the reactor wall per unit area, $\rho$ is the fluid density, $q'''$ is the volumetric heat generation term from the reacting flow, $C_p$ is the specific heat, $u$ is the fluid velocity in the x direction, and $D$ is the diameter of the reactor. The heat transfer is dominated by convective flows from the walls [18]. For tubular reactors, it has been found that the ratio of diameter to length of the reactor

plays a strong effect on reactor performance, primarily due to improved heat transfer [19]. As well, the influence of flow disturbance and other efforts to decrease the characteristic length scale inside the reactor have been shown to improve heat transfer [17, 20]. Acoustics have also been used by some researchers to improve heat transfer [21]. Both monolith and pelletized beds have been explored for steam reforming of methane, but commercial processing of methane is done with pelletized beds. Heat transfer for a pelletized bed can be determined using empirical relations, and has been studied extensively for both reacting and non reacting flows. Shown in Equation 2.11 is a Nusselt number relation as a function of Reynold's number[22]:

$$Nu \cdot \exp(\frac{6d_{catalyst}}{d} = 1.26Re^{0.95} \tag{2.11}$$

The overall convective heat transfer coefficient can be estimated using the correlation described above in Equation 2.11, and the characteristic time for heat transfer can be described as

$$\tau_{HT} = \frac{\Delta\bar{h}_{RXN}}{\dot{Q}} \tag{2.12}$$

where $\Delta\bar{h_{RXN}}$ is dependent on the fuel and the steam to carbon ratio, and can be determined by Equation 2.1, and $\dot{Q}$ is the heat transfer in to the steam reformer[15].

#### 2.1.3.2 Mass Transfer

Another rate limiting step is the mass transfer of the species within the system. This is both the bulk mass transfer controlled by flow patterns within the reactor, and the diffusion of species through the catalyst and boundary layer. The characteristic time for bulk mass transfer, like the heat transfer, is dependent on the dominant length scale and is a function of *Re*, as well as *Sc* [23]:

$$Sh' = 1.0(Re')^{1/2}Sc^{1/3} \tag{2.13}$$

$$Sh' = \frac{k_c d_{cat}\epsilon}{D\gamma(1-\epsilon)} \tag{2.14}$$

$$Re' = \frac{V d_{cat}}{\nu(1-\epsilon)} \tag{2.15}$$

where $D$ is the diffusivity, $\epsilon$ is the void fraction of the catalyst bed, and $\gamma$ is the shape factor, defined as the ratio of the catalyst surface area divided by the surface area of a spherical particle of the same effective diameter $d_{cat}$. The prime on the Sherwood and Reynold's number denotes the deviation from standard form to take into account the void fraction $\epsilon$ and shape factor $\gamma$. It can be seen that by increasing the shape factor $\gamma$ or decreasing the effective diameter $d_{cat}$ the bulk mass transfer can be improved. For systems that have fast kinetics, systems with very short characteristic lengths have been used to improve mass transfer such as with screens or very short monoliths[24].

Internal diffusion is a function of the concentration of species at the surface of the catalyst $C_{AS}$, the reaction rate $k$, combined Knudsen and external diffusivity $D_C$ and catalyst size $R$, and can be described using the Thiele modulus (Equation 2.16), which relates diffusion time to reaction time.

$$\varphi = \sqrt{\frac{kR}{C_{AS}D_C}}/R \tag{2.16}$$

The characteristic time is taken to be as shown below for a packed bed from Bird et al. [25] as reported in Yoon [18],

$$\tau_{MT} = \frac{1}{N\pi d_{cat}^2 C_{AS} D_C}[1 - \varphi \coth \varphi] \tag{2.17}$$

In general, steam reforming systems tend to be heat transfer limited, while auto thermal systems tend to be mass transfer limited.

#### 2.1.3.3 Chemical Kinetics

The chemical kinetics are dependent on the catalyst and the species involved, and are functions of partial pressure and temperature. The kinetics of various catalyst chemistries,

including $Ni$, in wide industrial use have been studied extensively [12, 13, 26]. The rate equations for chemical equations 2.2, 2.3, and 2.4 as reported by Xu and Froment [13] are

$$
\begin{aligned}
r_{SR} &= \frac{k_{SR}}{p_{H_2}^{2.5}}(p_{CH_4}p_{H_2O} - \frac{p_{H_2}^3 p_{CO}}{K_{SR}})/(DEN)^2 \\
r_{WGS} &= \frac{k_{WGS}}{p_{H_2}}(p_{CO}p_{H_2O} - \frac{p_{H_2}p_{CO_2}}{K_{WGS}})/(DEN)^2 \\
r_{DSR} &= \frac{k_{DSR}}{p_{H_2}^{3.5}}(p_{CH_4}p_{H_2O}^2 - \frac{p_{H_2}^4 p_{CO_2}}{K_{DSR}})/(DEN)^2 \\
DEN &= 1 + K_{CO}p_{CO} + K_{H_2}p_{H_2} + K_{CH_4}p_{CH_4} + K_{H_2O}p_{H_2O}/p_{H_2}
\end{aligned}
$$

in which each of the rate coefficients $k_i$ and adsorbtion constants $K_j$ is of the form

$$
\begin{aligned}
k_i &= A_i \exp \frac{E_{ai}}{RT} & i &= SR,\ WGS,\ DSR \\
K_j &= A_j \exp \frac{\Delta H_j}{RT} & j &= CO,\ H_2,\ CH_4,\ H_2O
\end{aligned}
$$

Formation rates for $CO$ and $CO_2$ and the disappearance rate of $CH_4$ can then be described as

$$r_{CO} = r_{SR} - r_{WGS} \tag{2.18}$$

$$r_{CO_2} = r_{WGS} + r_{DSR} \tag{2.19}$$

$$r_{CH_4} = r_{SR} + r_{DSR} \tag{2.20}$$

The time constant for chemical kinetics can be shown as

$$\tau_{CK} = \frac{5}{k} \tag{2.21}$$

as a first order system is assumed to reach its final value after five time constants have passed [17]. The rate limiting step is the decomposition of methane so the chemical kinetics can be considered to be dominated by Equation 2.20.

All three factors of heat transfer, mass transfer, and chemical kinetics are linked, where geometry and flow rate changes affect heat and mass transfer, which affects catalyst activity. Steam reforming, due to the highly endothermic nature of the dominant reactions Equations 2.2 and 2.4 and because heat is supplied externally, is typically heat transfer limited.

### 2.1.4 Catalyst Degradation

Over time, and particularly with use of high sulfur feedstocks or low steam to carbon ratios, the catalyst becomes deactivated, due to chemical poisoning, physical blockage, and other reductions of available sites [27, 28]. Degradation of the catalyst bed can be minimized through operating conditions, and some activity can be recovered through regeneration [28–30]. Other degradation, such as sulfur poisoning or sintering, cause permanent loss of activity on the catalyst and manifest as a reduction in conversion over time.

#### 2.1.4.1 Coking

Coking, or the formation of solid carbon in the catalyst bed, is an ongoing problem in steam reforming by blocking active sites and clogging filters, valves, and restrictions. There are several pathways to the formation of soot and coking of the catalyst. The reactions involved include thermal cracking of the fuel to produce hydrogen and carbon, and the dissociation of hydrocarbons on the surface of the catalyst [14, 31]. Two dominating reactions for the reforming of methane are shown below.

$$CH_4 \longleftrightarrow C + 2H_2 \tag{2.22}$$

$$C_nH_{2n+2} \longleftrightarrow nC + (n+1)H_2 \tag{2.23}$$

Control of coking on the surface of the catalyst can be thought of as a balance between coke generation, and coke gasification. There are both reactions in the gas phase and at the surface of the catalyst. Gas phase reactions include thermal cracking and the production of polycyclic aromatic compounds from free radicals, which have been identified as soot and coking precursors [29–31]. The thermal cracking of the fuel can be mostly avoided by

limiting the preheat temperature. The gas phase reactions allow a calculation of a S/C ratio where no soot or coke is formed [14], however these methods estimate a high S/C ratio, with a corresponding reduction in efficiency due to the heating of additional water that is unreacted. These gas phase reactions, through a free radical process, produce polymers, tars, and coke [28]. These intermediates can then condense on the surface of the catalyst, and become a major source of coke. These intermediates can be minimized by control of the gas phase reactions in the form of dilution by steam, or minimization of the heated space.

The most important reactions to control are those at the surface of the catalyst, where coke formation blocks active sites and causes increased pressure drop across the reactor. According to Skjøth-Rasmussen [31] and Trimm [14], hydrocarbons dissociate on the catalyst surface to form a highly reactive carbon species, most of which is gasified but some of which rearranges on the surface to form carbon structures more resistant to gasification. This pathway is particularly important in relatively low temperature steam reforming with liquid fuels, where the fuel can condense on the surface of the catalyst [18]. To minimize catalyst deactivation due to coking, it is important to gasify the carbon on the surface while still in its highly active state and before it polymerizes into more stable forms. This necessitates a high mass transfer rate to allow diffusion of reactants to the catalyst surface to gasify the coke [30]. Mass transfer directly affects local stoichiometry. It is well known that the coking limit of diffusion flames is dependent on burner design [31], and has been shown that mixing affects conversion in autothermal reforming. Good mixing is an important consideration, as is the minimization of boundary layers, to avoid coking. Even though the global balance may be correct, there is no guarantee that local stoichiometry will be, and these zones can generate soot because of this imbalance with respect to the global levels. The dependence of coking on temperature is roughly bell shaped as can be seen in Figure 2.1, and the low temperature side of the distribution is driven by formation kinetics of soot precursors. There is also a dependence on pressure, in which low pressure inhibits sooting and high pressure promotes it; and fuel partial pressure, which similarly positively affects soot formation [31].

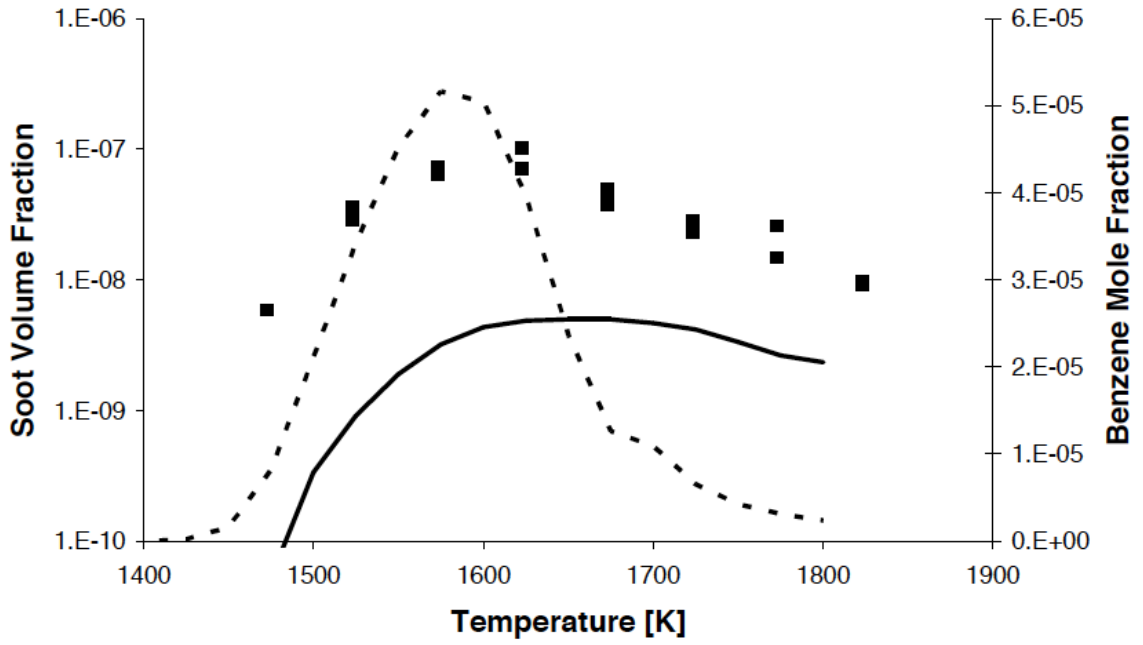


Figure 2.1: Comparison between the soot volume fraction determined by sampling of particles on aerosol filters (points), and model calculations (lines) of the concentration of benzene in the gas phase (dashed line) and the volume fraction of soot (full line) [31]

Coke formation can be detected in practice when a large pressure drop builds through the reactor. As well, soot particles collect downstream of the reactor and cause blockages. Coke formation on catalysts can be measured in a variety of ways. The most common is through thermogravimetric analysis [30], but this is inconvenient for repeated studies utilizing a relatively large fixed bed reactor. Others have introduced an oxidizer to the coked catalyst and use a gas analyzer at the conclusion of a fuel reforming experiment to measure $CO_2$ and $CO$ levels until they drop and stabilize. Others have investigated the use of electrical resistance [32] and microwave resonance [33, 34] to detect the coke load *in situ*.

#### 2.1.4.2 Sintering

Catalyst active sites can fuse with other sites, forming larger metallic particles which reduces the total number of available types [27]. The reduction in activity is permanent. Sintering has been found to be highly temperature dependent. There are two mechanisms described by Sehested [27] for this metallic particle growth. By limiting peak temperatures

and keeping partial pressures in desirable ranges as suggested by Sehested [27] the effect of sintering on activity can be kept to a minimum.

#### 2.1.4.3 Fouling

Catalyst pellets can be deactivated by fouling from residues in the fuel feed. Both Skjøth-Rasmussen [31] and Trimm [14] point to this pathway, as well as Yoon [18], for liquid fuels to form tar like solids on catalyst surfaces, both from low temperature coke forming reactions on the catalyst surface and from heavier hydrocarbons in the fuel itself. However, other gas phase pathways exist for the formation of polycyclic aromatic compounds that are precursors to soot and other heavier carbon structures. This soot can then cause blockage of the active sites. As well, empty heated space can give rise to solid carbon which can physically block catalyst sites and downstream filters and restrictions.

### 2.1.5 Modeling

The steam reforming reactor can be modeled as a system of first order differential equations, as other parties have demonstrated [12, 31, 35, 36], with appropriate correlations for the heat and mass transfer and chemical kinetics. These models have been found to be in good agreement with experimental data [12, 35] and can be used as a design tool for reactor sizing. For the purpose of sizing a reactor for this study, degradation effects were not included in the model of the steam reformer.

## 2.2 Spark Ignition Engines

Spark ignition engines play a large role in our energy systems. The Otto cycle engine is the most widely used cycle in transportation systems.

### 2.2.1 Fundamentals

A four stroke internal combustion engine has four distinct modes: intake, in which air and fuel are drawn in to the cylinder; compression, in which the fuel/air mixture is compressed; expansion, in which the hot gases are expanded and work is extracted; and exhaust, in which the burnt, spent gases are ejected and the cylinder is cleared for the next charge.

In Figure 2.2, $Q_{in}$ is shown as an isochoric process, and both compression and ex-

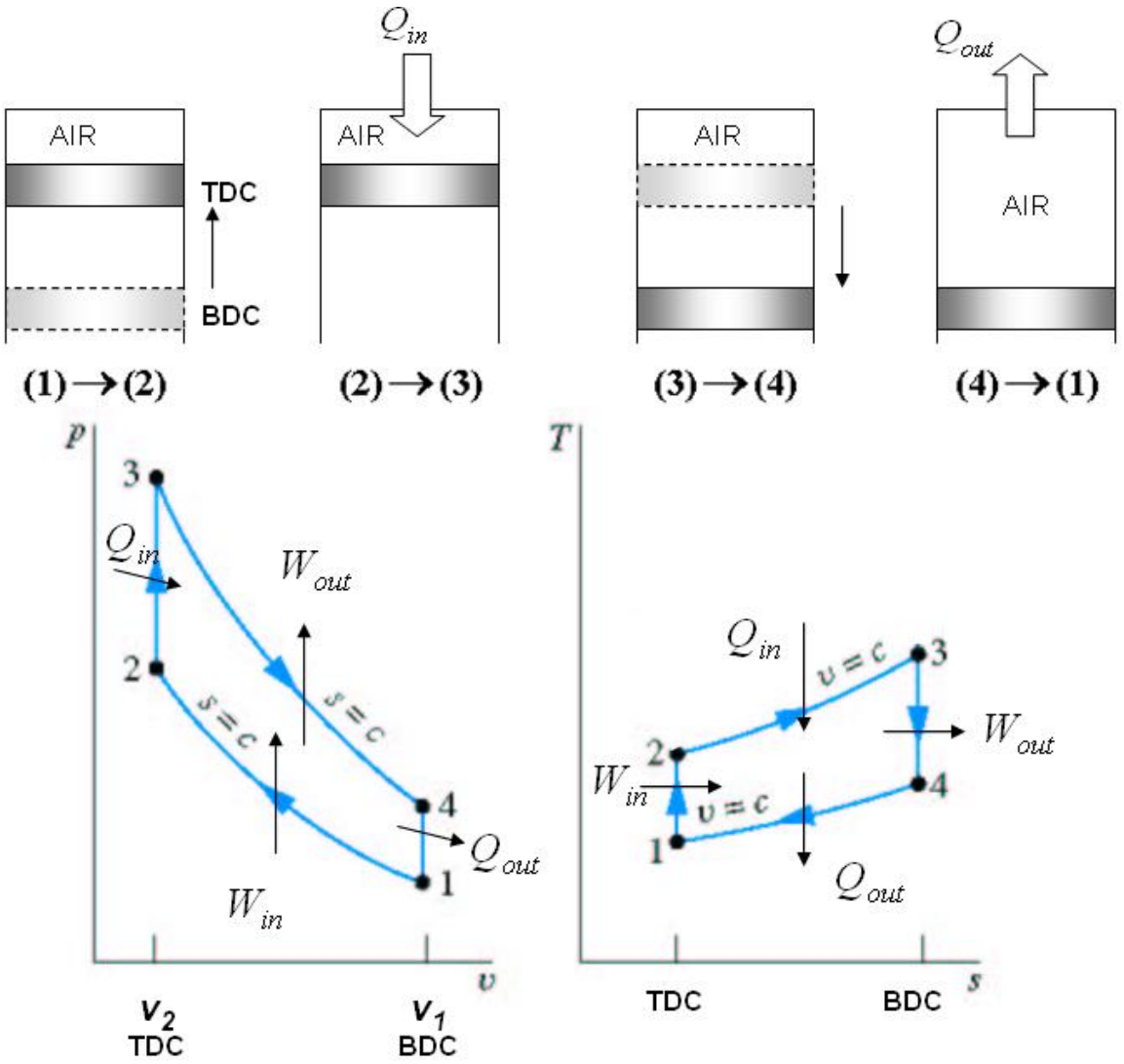


Figure 2.2: Idealized Otto Cycle

pansion are shown as isentropic processes. $Q_{out}$ is the heat rejected in the exhaust. The thermal efficiency in an idealized engine from a theoretical standpoint is only governed by two factors, the compression ratio and the ratio of specific heats.

$$\eta = 1 - (\frac{1}{r^{(\gamma-1)}}) \tag{2.24}$$

The compression ratio is the ratio of volumes from the greatest volume to the smallest volume in the cylinder. The ratio of specific heats, $Cp$ and $Cv$, or $\gamma$, is usually taken to be 1.4 for air at 0°C: this is known as the cold air standard assumption. This represents a

peak theoretical efficiency for an Otto cycle engine, but real cycles differ from this due to heat transfer, non-instantaneous heat release, and deviations from the ideal assumptions such as a different $\gamma$ for compression and expansion strokes.

### 2.2.2 Stoichiometry

The combustion stoichiometry for a generalized hydrocarbon fuel can be described as

$$C_\alpha H_\beta + (\alpha + \frac{\beta}{4})(O_2 + 3.76N_2) \longrightarrow \alpha CO_2 + \frac{\beta}{2}H_2O + (\alpha + \frac{\beta}{4})3.76N_2 \tag{2.25}$$

Combustion stoichiometry affects the internal combustion engine by changing the heat release rate, $\gamma$, and the power output of the engine [1]. Leaner combustion stoichiometry generally positively affects thermal efficiency, due to more complete combustion and a higher specific heat for the expansion stroke, but there are limitations on the leanness of the charge based on the fuel properties.

#### 2.2.2.1 Lean Stability Limit

There is a point at which an engine cannot run leaner without a dramatic decrease in efficiency, due to misfire and incomplete burning [1]. The cycle to cycle variation increases rapidly, and the engine will not run in a stable way. This is typically described by the *coefficient of variation in indicated mean effective pressure*. $COV_{imep}$ is expressed in Heywood [1] as:

$$COV_{imep} = \frac{\sigma_{imep}}{imep} \times 100 \tag{2.26}$$

A threshold value can be chosen for the stability limit, with 10% found to be a good guideline [1]. However, this limit can be defined in any way that is practical. As the cycle to cycle variation increases the average torque output at a given engine speed will decrease, and output power will fall. The resulting decrease in brake thermal efficiency $\eta_{TH}$ can be compared to some reference and a lean stability limit can be defined in these terms.

### 2.2.3 Exhaust Temperature

The temperature of the exhaust is dependent on the chemical energy added, the specific heat of the gas mix, the work extracted, and the heat loss through the cylinder walls. As seen in Figure 2.2, $Q_{out}$ for the ideal cycle is assumed to be only in the exhaust, but real engines transfer heat through the engine block and to other sinks. The exhaust temperature can be an indicator of the load on the engine, with higher load having a positive effect on exhaust temperature. As can be expected, there is a nearly linear proportionality with engine stoichiometry $\lambda$ and exhaust gas temperature, as within the stable range of $\lambda$ brake thermal efficiency $\eta_{TH}$ is relatively unchanged. Deviations from maximum brake torque spark timing also result in a positive effect on exhaust temperature, as less work is extracted.

### 2.2.4 Emissions

Emissions from an internal combustion engine are primarily $CO_2$, $NO_X$, and hydrocarbons ($HC$). These can vary based on the operating point of the engine and are strongly dependent on $\lambda$. For values of $\lambda$ greater than unity, hydrocarbon emissions are very low, but can be significant during rich operation or during warm up, where flame quenching on cylinder walls can allow unburned hydrocarbons to pass through. Similarly, $CO$ emissions are quite low with lean combustion, and are typically only present in significant amounts during rich combustion. Both $HC$ and $CO$ emissions rapidly rise near the lean stability limit, due to the incomplete burning present at those operating conditions. Figure 2.3 shows this relationship between the inverse of $\lambda$, the fuel air equivalence ratio $\phi$, and these three pollutants as general trends.

### 2.2.5 Ignition Timing

Ignition timing, measured in degrees before top dead center (°BTDC), affects the efficiency and the stability of the engine. Maximum efficiency demands that the spark timing be set such that at a particular RPM the torque output is maximized (MBT). Maximum torque is developed when maximum pressure is developed just after top dead center (TDC). The combustion process takes some small amount of time, dependent largely on the fuel

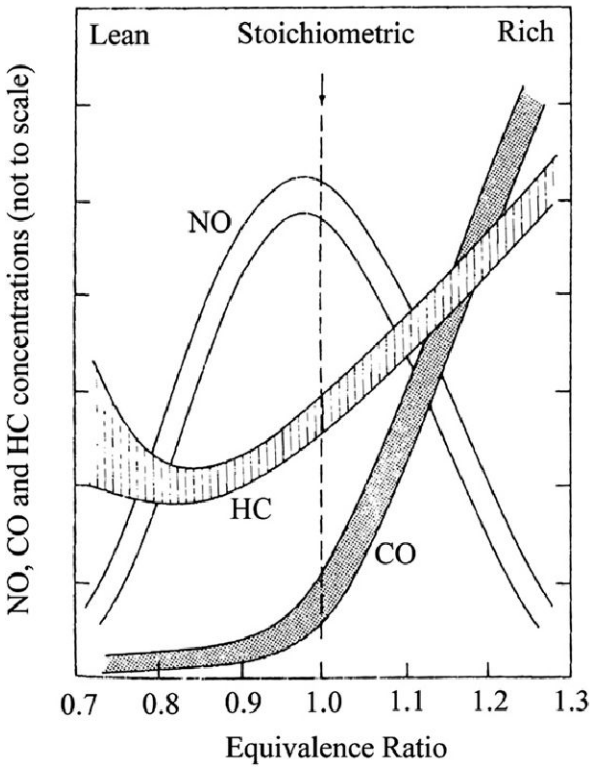


Figure 2.3: Emissions as a Function of fuel air equivalence ratio $\phi$ [1]

type and the stoichiometry. It is initiated before the end of the compression stroke, and ends after peak cylinder pressure is reached. If the combustion is initiated too early by advancing the timing, then the compression stroke work transfer from the piston to the gas increases, and output torque decreases. If the combustion event is initiated too late, then the peak cylinder pressure occurs later in the expansion stroke and is reduced in magnitude, resulting in decreased work transfer from the cylinder gases to the piston and therefore lower output torque. Maximum brake torque spark timing, or MBT spark timing, occurs when the magnitudes of these opposing trends oppose each other[1]. The overall burn angle, or $\Delta\theta_o$, is a way of describing the combustion process in terms of how much of the engine cycle the combustion process occupies. It is composed of two pieces, the flame development angle $\Delta\theta_d$ and the rapid burning angle $\Delta\theta_b$. The former is the crank angle interval in which the combustion process is initiated and a small fraction (usually 10%) of the fuel chemical energy has been released. The latter is the crank angle interval in which the bulk of the charge is burned, between $\Delta\theta_d$ and the end of the flame

propagation process when the charge is 90% consumed.

Stoichiometry affects flame speed, and heat release rate, which changes the burn angle $\Delta\theta_o$. This directly affects MBT spark timing. As well, different fuels have different flame speeds and heat release rates, which also affect $\Delta\theta_o$ and therefore MBT spark timing. Any study of engine performance examining the effect of composition and stoichiometry must also adjust the spark timing to account for these differences.

### 2.2.6 Hydrogen Assisted Combustion

The addition of hydrogen allows leaner combustion than other fuels, which reduces the incidence of pollutants and can improve efficiency [4, 8, 37–39].This is due to more complete combustion, fewer unburned hydrocarbons, lower combustion temperatures, and reduced heat transfer to the cylinder walls. However, hydrogen enrichment does not uniformly lead to more efficient engine operation, as can be seen in Figure 2.4, and can depend on $\lambda$, cylinder geometry, compression ratio, and spark timing.

The number of experiments and modeling attempts on the combustion process of hydrogen enriched hydrocarbon are extensive, and hydrogen's fundamental combustion properties are responsible for the effects found with enrichment, including increased flame speed, reduced pollutant formation, and an extended lean flammability limit [40–44].

Figure 2.5 shows the extension of the lean limit with the addition of $H_2$, as well as brake specific $NO_x$ emissions by fuel composition and equivalence ratio $\phi$. Notice that $NO_x$ emissions are higher at the same equivalence ratio for the hydrogen blends. Emissions can be reduced to zero emission vehicle specifications with a 30% $H_2$, 70% $CH_4$ blend, provided it is operated in lean conditions [45].

#### 2.2.6.1 Flame speed

Hydrogen affects the combustion process in several ways. The high laminar flame speed of hydrogen increases the heat release rate. The reduced burn angle means that the actual engine performance is closer to the idealized Otto cycle with isochoric heat release. Because of this, the addition of $H_2$ has an effect on MBT spark timing at a given engine RPM; the timing must be retarded to account for the greater burn rate.

Figure 2.6 shows a pressure trace for different fuels at stoichiometric $\lambda$ values and a

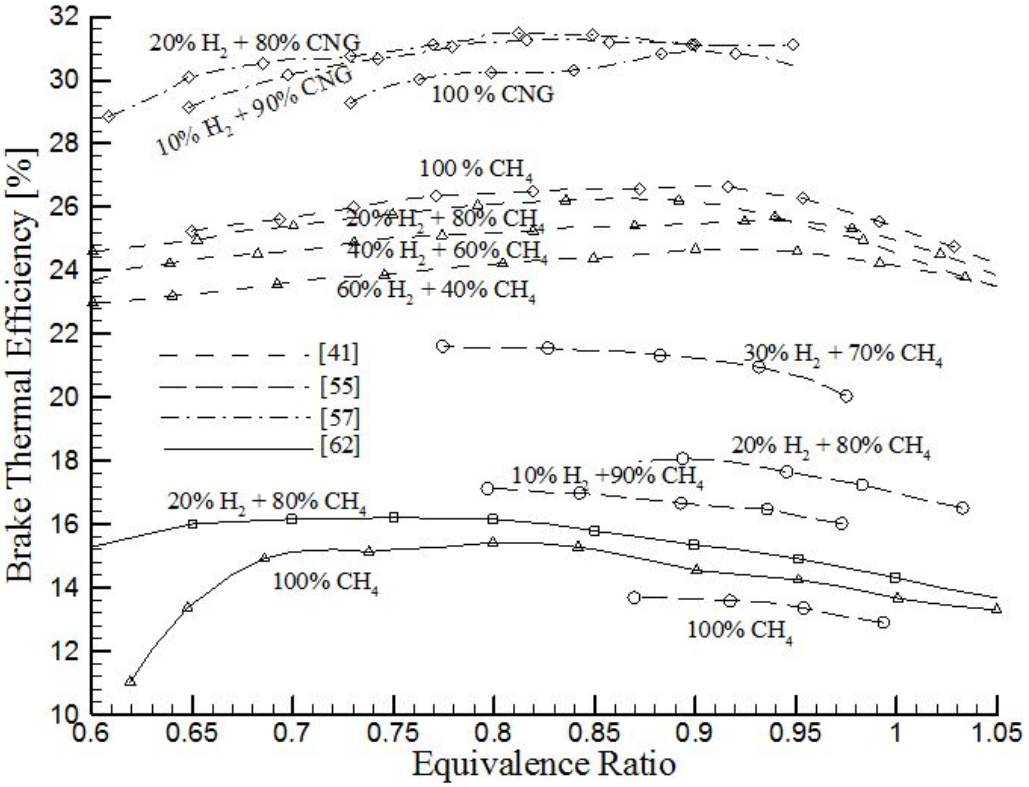


Figure 2.4: Brake Thermal Efficiency vs. Equivalence ratio $\phi$ [2]

constant spark timing. As can be seen, the pressure develops faster and the peak is higher for the mixtures with $H_2$ than $CH_4$ alone.

Radicals are generated at a greater rate with greater concentrations of hydrogen [1, 46]. Greater radical concentration affects the combustion process by extending the lean stability limit [42, 47, 48] and shortening the flame nucleation period thus increasing heat release rate [42]. Increased heat release rate in internal combustion engines increases efficiency, reduces cycle to cycle variability, and extends the lean stability limit [1].

#### 2.2.6.2 Lean Stability Limit

The increased flammability limit of hydrogen allows a greater operating range in terms of $\lambda$. The high flame speed of hydrogen can be attributed to its high diffusivity, its high thermal conductivity, and the concentration of radicals. A higher flame speed ensures more complete combustion and fewer instances of misfire [1].

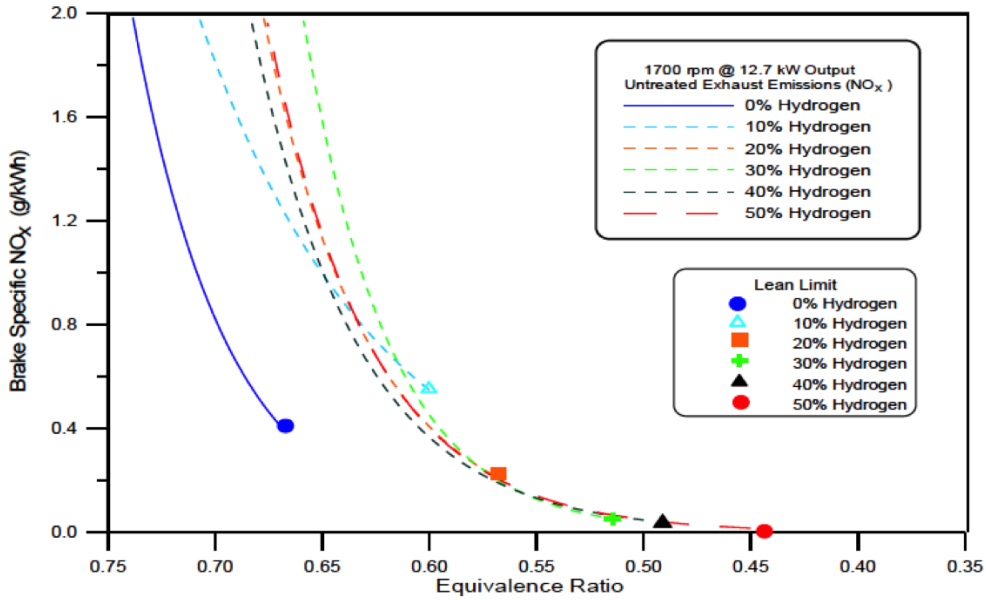


Figure 2.5: Brake Specific $NO_x$ vs. Equivalence Ratio $\phi$

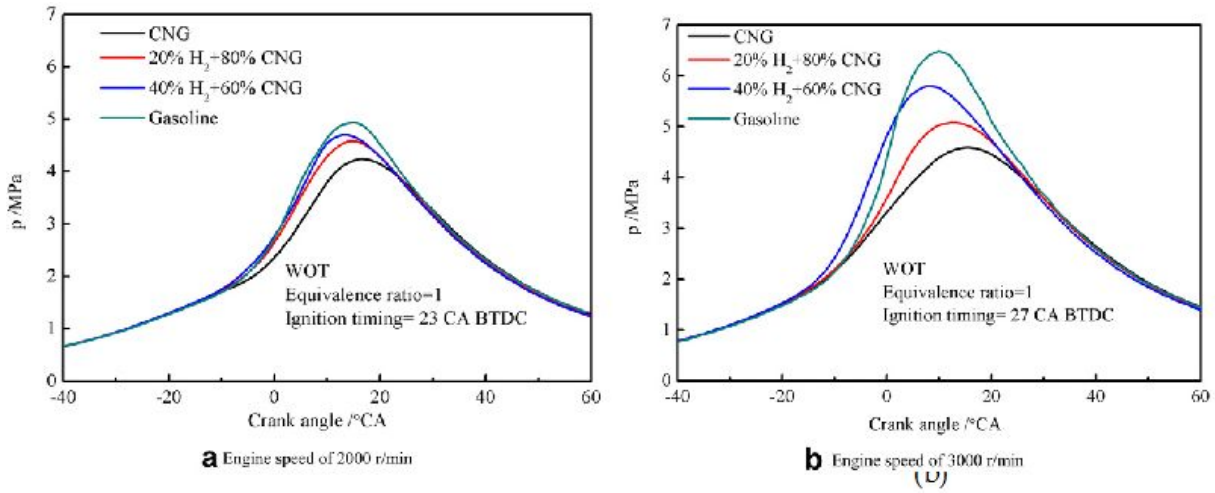


Figure 2.6: In Cylinder Pressure vs. Crank Angle for different Fuels [3]

Hydrogen addition increases the lean stability limit with a variety of fuels in a nonlinear way; a small addition of hydrogen can have a large effect on the lean stability limit [8]. Moderately lean equivalence ratios yield higher efficiencies than stoichiometric, due to excess oxygen to support complete combustion, but efficiency at the lean stability limit is reduced due to decreased heat release rate and increases in cycle to cycle variations [1].

The addition of hydrogen extends the lean limit and reduces cycle to cycle variations. Lean operation improves efficiency by reducing heat losses to the cylinder walls, reducing dissociation of combustion products, and increasing the ratio of specific heats $\gamma$ during the expansion process [8]. Reductions in cycle to cycle variations improve spark timing for more cycles, improving efficiency [1].

Throttling reduces the total fuel air charge to the engine and enables part load output. Brake thermal efficiency is negatively impacted by charge throttling. However, by extending the lean limit the need to throttle is reduced, and power output can be reduced as low as 30% without throttling [8]. This can significantly reduce throttling losses in real drive cycles, where load demand can vary significantly.

## 2.3 Thermochemical Recuperation

Recognizing that there are few practical sources of stored hydrogen, and given that there are significant thermal resources available in the exhaust of an SI engine, an onboard generation system utilizing the thermal resource presents a good opportunity. In Thermochemical Recuperation (TCR) the process gasses are heated by the exhaust of the internal combustion engine. These process gases then recover the thermal energy as chemical energy, measured as a change in the heating value of the fuel stream. There has been some experimental work in TCR that utilizes methanol reformers to investigate lean burn operation of internal combustion engines [6, 49], but the steam reformer suffered from low conversions and selectivities. As well, there has been some work utilizing $Ni$ or Noble metal based catalysts for iso-octane and other fuel steam reforming in a TCR system, as well as autothermal reforming [8, 44, 50–53], but most studies did not experimentally examine the full system, and restricted themselves to the hydrogen generator component. Similarly, there have been numerous studies on the effect of hydrogen or syngas in internal combustion engines alluding to the possibility of it being supplied from an on board source, but the experimental work utilized a bottled source of hydrogen or syngas.

### 2.3.1 Thermal Considerations

Exhaust heat recovery is of prime concern in a thermochemical recuperation system. Lower $\lambda$ values yield higher exhaust gas temperatures, increasing the available heat for steam reforming. Higher exhaust temperatures allow for increased flow through the steam reformer without a drop off in performance due to thermal limitations, and allows for greater hydrogen percentages in the engine fuel stream. Leaner operation of the engine results in lower exhaust gas temperatures, which limits the maximum flow of reactants through the steam reformer to maintain high conversion. Most investigations into TCR have utilized either autothermal or partial oxidation fuel reforming processes to avoid these thermal considerations, as highly variable engine loads produce a highly variable thermal resource and an oxidative reforming process is less sensitive due to the reduced endothermicity [8, 44, 50, 54].

### 2.3.2 Chemical Considerations

Greater concentrations of $H_2$ in the fuel stream can have a slight effect on exhaust gas temperatures of spark ignition engines. The power output of internal combustion engines is reduced at stoichiometric air to fuel ratios with the addition of $H_2$ to the fuel stream, due to reduced volumetric energy content. High concentrations of $H_2$ allow the engine to be run stably at much higher $\lambda$ values, which reduces $NO_x$ and $HC$ emissions due to lower peak temperatures and more complete combustion, respectively.

Steam reforming rates are higher at higher temperatures. The efficiency of the steam reforming process, and the composition of the product stream, is dependent on the temperature of the catalyst bed. As well, the process is affected by the $S/C$ ratio, which generally has a positive effect on $H_2$ yield but a negative effect on overall efficiency, due to greater heating load for unreacted water and a reduced selectivity for $CO$.

Most prior work in TCR has focused on generating $H_2$ rich effluent from oxidative steam reforming fuel processors. The oxidizer for practical on board systems is air, which results in a dilution of the products and thermal resource [4, 44, 54]. Heavier, longer chained hydrocarbons such as iso-octane, heptane, and JP-8 have been explored as well in proposed TCR systems due to the practicality presented by their energy density and

current presence in transportation systems. However, these have lower hydrogen selectivities, have greater $CO_2$ dilution, and typically require greater $S/C$ ratios to prevent the coking and subsequent deactivation of the catalyst, all which have a negative effect on overall system performance [26, 31, 53]

### 2.3.3 Measures of Efficiency

There are several ways that efficiency can be considered, and it is dependent on whether the system in question should be evaluated as a component or as a complete system.

#### 2.3.3.1 Engine

When evaluating the engine/generator system, one way to determine the efficiency is to measure the electrical power out and the fuel energy going in, giving the brake thermal efficiency of the system. This is shown below in Equation 2.27.

$$\eta_{TH} = \frac{\dot{E}}{\dot{m}_{Fuel} \times LHV_{Fuel}} \tag{2.27}$$

where $\dot{E}$ is the power from the generator, and $\dot{m}_{Fuel}$ and $LHV_{Fuel}$ are the mass flow rate and specific energy content of the fuel, respectively. As it is not practical in this case, nor entirely relevant, the brake thermal efficiency is used over the indicated thermal efficiency. Frictional losses, conversion losses, and similar can be ignored as they are not expected to change significantly from one fuel to the next.

#### 2.3.3.2 Steam Reformer

For a steam reformer, several methods of evaluation are available. As described in [11], the method of analysis depends on the system being evaluated. and whether the reactor is considered a component or the complete system. For a plant producing hydrogen for industrial processes, it is sensible to treat the steam reformer efficiency as the quotient of the flow rate of the desired products times the heating value, and the sum of the fuel and externally supplied heat.

$$\eta_{SR} = \frac{\dot{m_{H_2}} \times LHV_{H_2}}{\dot{m_{Fuel}} \times LHV_{Fuel} + Q_{In}} \tag{2.28}$$

This is intuitive as there is a cost to producing the reformate stream due to the

endothermic nature of the reaction. However, it is not appropriate to consider the steam reformer this way as the process heat is waste heat. As well, the goal is not to produce a specific product ($H_2$) but to improve the heating value of the fuel, so the chemical potential of other species can be considered when evaluating the performance of the steam reformer. A better definition of the efficiency of the steam reformer, when considered as a component of the TCR system, is that of Equation 2.7, which allows greater than unity efficiencies.

#### 2.3.3.3 Heat Exchanger

Though heat utilized in a TCR system is recovered and would otherwise be wasted, it is still important to characterize the efficiency of the heat exchange process. The efficiency of the heat exchanger is defined in Equation 2.29 as

$$\eta_{HX} = \frac{\Delta h_{SR} \dot{m}_{SR}}{\Delta h_{EX} \dot{m}_{EX}} \tag{2.29}$$

in which $\Delta h_{SR}$ is the enthalpy change of the process gases, $\Delta h_{EX}$ is the enthalpy change of the exhaust across the heat exchanger, and $\dot{m}_{SR}$ and $\dot{m}_{EX}$ are the mass flow rates through the steam reformer and of the exhaust, respectively.

#### 2.3.3.4 Closed Loop Thermochemical Recuperation

A diagram of the thermal efficiency of the closed loop TCR system can be seen in Figure 2.7. In this diagram it can be clearly seen that on a thermal efficiency standpoint there would be no reason to use a TCR system if there were not fuel reformer efficiencies greater than 100%. As autothermal fuel reformer schemes consume a portion of the fuel to sustain the reaction, these systems cannot improve efficiency based on energy recovery alone.

The complete system, then, has the global efficiency as shown in Equation 2.30:

$$\eta_{SYS} = \frac{\eta_{TH}}{1 - x + \frac{x}{\eta_{SR}}} \tag{2.30}$$

in which $\eta_{TH}$ is the thermal efficiency of the engine, $x$ is the fraction of fuel reformed, and $\eta_{SR}$ is the efficiency of the steam reformer as defined in Equation 2.7. However, for practicality this can be measured as shown in Equation 2.31 as these measurements are at the system borders.

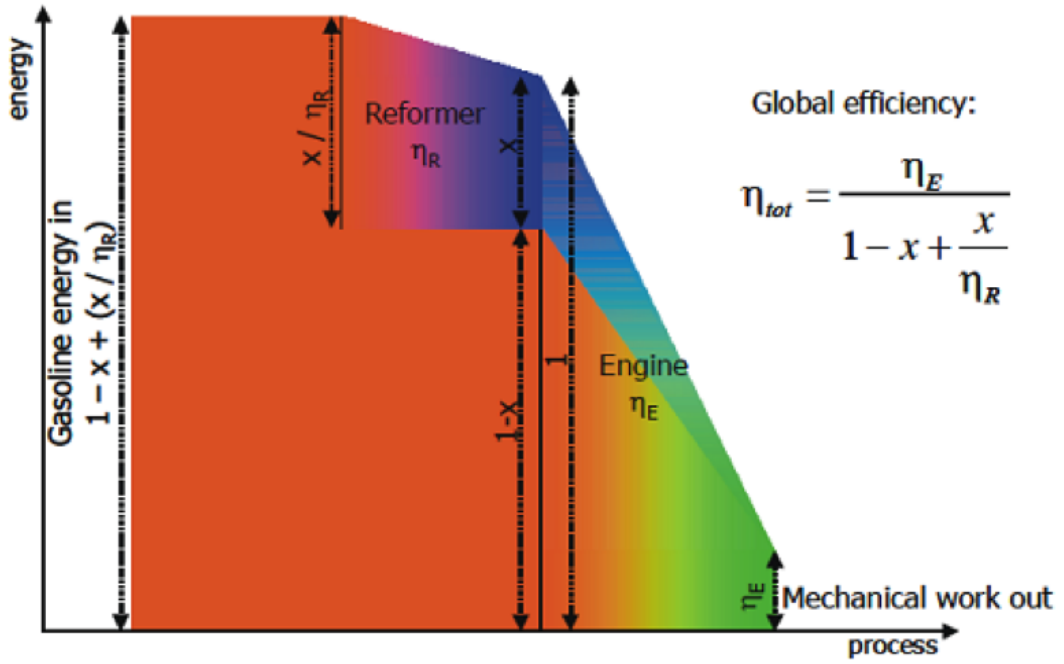


Figure 2.7: System Efficiency of a gasoline fueled engine with Thermochemical Recuperation

$$\eta_{SYS} = \frac{\dot{E}}{(\dot{m}_E + \dot{m}_{SR}) \times LHV_{Fuel}} \tag{2.31}$$

where $\dot{E}$ is the electrical power generated, $\dot{m}_E$ is the mass flow rate of virgin fuel to the engine, $\dot{m}_{SR}$ is the mass flow rate to the steam reformer, and $LHV_{Fuel}$ is the heating value of the fuel, lower value. As can be seen the complete engine and TCR system can be analyzed using this last definition presented in Equation 2.31, in which the system boundaries are expanded to include the engine subsystem. The energy inflows are then just the fuel energy in and the energy outflow is the electrical power from the generator. Any parasitic loads such as reactant preheating, pumping loads for reactants or coolant are neglected in this study, but represent a small fraction of total energy inputs.

## 2.4 Contribution

This work will experimentally investigate closed loop thermochemical recuperation, by observing the relationship between thermal efficiency, normalized air fuel equivalence ratio $\lambda$, and the percentage of the fuel stream diverted to the steam reformer. The

goals are recovery of exhaust heat energy through steam reforming, demonstration of an on board hydrogen source for an internal combustion engine, and extension of the lean limit using raw reformer products. This is done with the use of a small, single cylinder 4-stroke engine attached to an electric generator that provides a brake, and a custom built chemical reactor and heat exchanger unit.

# Chapter 3

# Experimental Facility and Approach

The experimental work was completed using a custom built steam reformer and heat exchanger attached to the exhaust system of a commercially available single cylinder naturally aspirated gas fueled engine. A system schematic is shown in Figure 3.1.

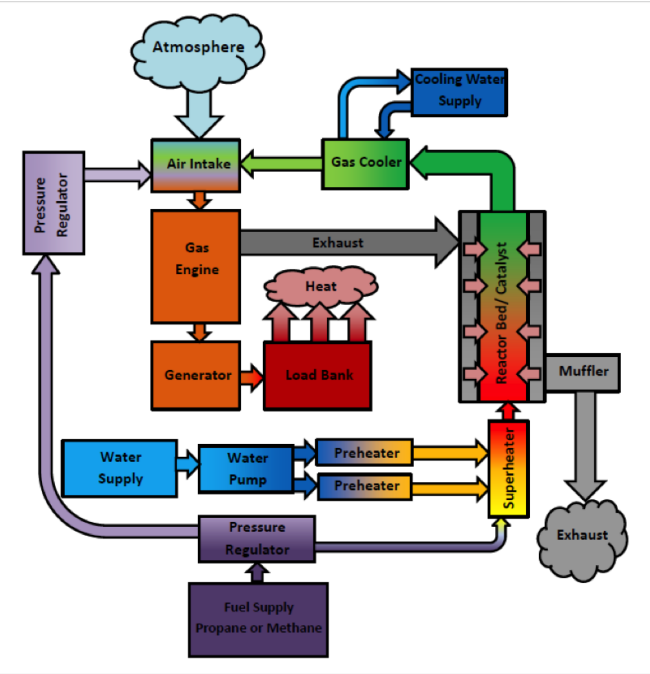


Figure 3.1: Schematic of the Thermochemical Recuperation Experimental apparatus

## 3.1 Engine

The power plant in use is a overhead valve type single cylinder 4-stroke engine/generator combination manufactured for Generac®. The engine is rated at 7kW for propane ($C_3H_8$) and 6kW for methane ($CH_4$). It is designed for emergency and standby operation in a home environment. It has a mechanical governor that is tunable for different engine speed set points, by way of an adjustable nut.

### 3.1.1 Ignition System

Critical to a study of hydrogen enrichment and variable combustion stochiometry is the ability to vary spark timing. This was done with a MSD brand single cylinder programmable ignition part number 4217, which interfaced via a RS-232 serial connection to the computer. It has 1°crank angle (CA) of resolution and was intended for use on a motorcycle or motor scooter. The factory ignition system was disabled. A schematic of the system is shown in Figure 3.2.

Timing is confirmed by use of an analog strobe inductive timing light. An indicator was affixed to the flywheel and a protractor was positioned above it, allowing actual spark timing to be read with the timing light.

### 3.1.2 Engine Stoichiometry

Engine combustion stoichiometry, $\lambda$, was measured by a Bosch wideband $O_2$ sensor designed for automotive use, model number LSU 4.9. The specifications are shown below.

Table 3.1: Bosch LSU 4.9 Specifications

| | |
|---|---|
| Exhaust Gas Temperature (operating) | $< 930$°C |
| Exhaust Gas Temperature (max) | $< 1{,}030$°C |
| Exhaust Gas Pressure | $< 4$ bar |
| $\lambda$ Measurement Range | 0.65 - Free Air |

The sensor was controlled with a $\lambda$ sensor controller by ALM which allowed for programmable voltage output for a range of $\lambda$ values.

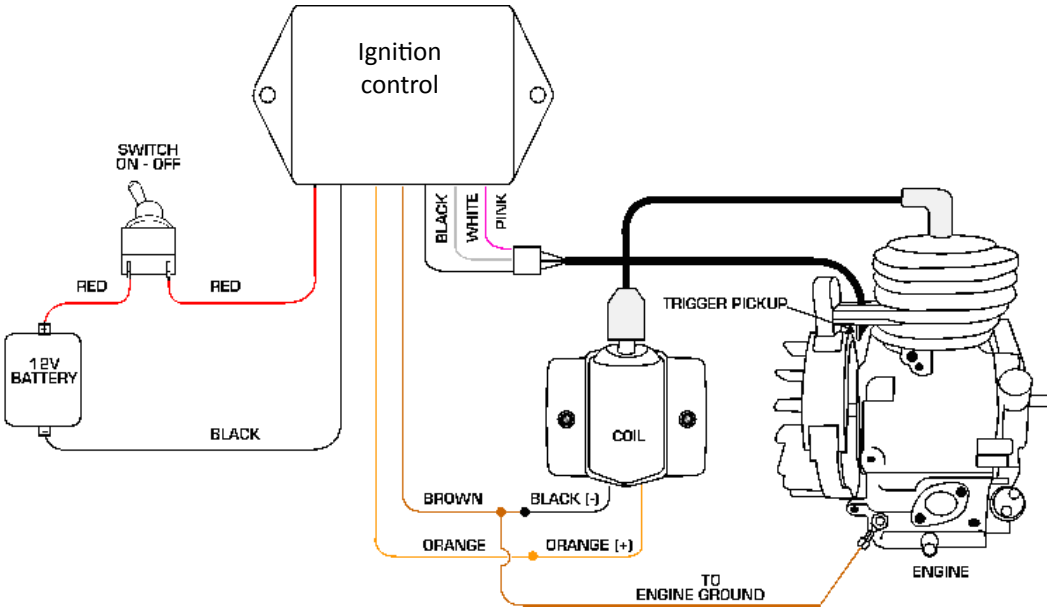


Figure 3.2: Ignition System Schematic

Stoichiometry was adjusted through two needle valves to control fuel flow. One needle valve was located just before the venturi and controls the virgin fuel flow and the analysis return line. This valve replaced the standard issue orifice, which was designed for constant stoichiometry. The second needle valve was located at the outlet of the syngas cooler.

### 3.1.3 Load Bank

To provide the load to keep the engine at a desired speed for a particular throttle position, several commercially available heaters were used. These heaters were each rated between 1000 - 1500W, and were connected to a circuit breaker bank provided with the generator. The power through these heaters was controlled using two Crydom phase control modules. The load is adjusted to maintain 3600 RPM for 60Hz power with a PID loop. A schematic is shown in Figure 3.3.

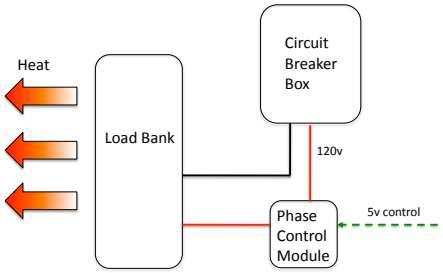


Figure 3.3: Load Bank Schematic

## 3.2 Steam Reformer

The steam reformer is a 0.9m (3') long, 76mm (3") OD SS316 tube, 1.6mm (0.065") wall thickness, with a flange and cap on one end and a reducing cone and flange on the other. The pelletized catalyst bed is supported on several stainless steel screens fit into the reactor tube and held in place with a spring ring. The reactor is shrouded by a 101mm (4") OD SS304 tube, 1.6mm (0.065") wall thickness, which composes the heat exchanger. The flanged caps are V band clamps designed for automotive use. They allowed easy access to the catalyst bed for diagnostic purposes and for replacement. The caps on either end were fitted with three compression fittings to allow for gas flow, pressure taps, and thermocouple placement. The flanges are sealed with a high temperature gasket sealant, Copaltite®, which provides a leak tight seal.

The entire reactor assembly is fit into the heat exchanger tube, the smaller reducing cone end inserted first through a snug fit end of the heat exchanger. The other end of the reactor is attached with a V band clamp to the heat exchanger at the top.

Temperature measurement was done at both ends of the steam reformer by a K type, stainless steel jacketed thermocouple inserted in 25mm (1") through the reactor end cap. A schematic of the steam reformer is shown in Figure 3.6.

Figure 3.4: Installed steam reformer, shown with thermocouples and inner thermal wrap insulation

Figure 3.5: Steam reformer and heat exchanger shell (L), and top detail (R)

### 3.2.1 Catalyst Bed

The catalyst bed was composed of a commercial pelletized catalyst, manufactured by Süd-Chemie. It is a low pressure drop nickel catalyst, Reformax 330, designed for use with methane-rich feedstocks.

The catalyst bed was located in the heated section of the steam reformer, and held

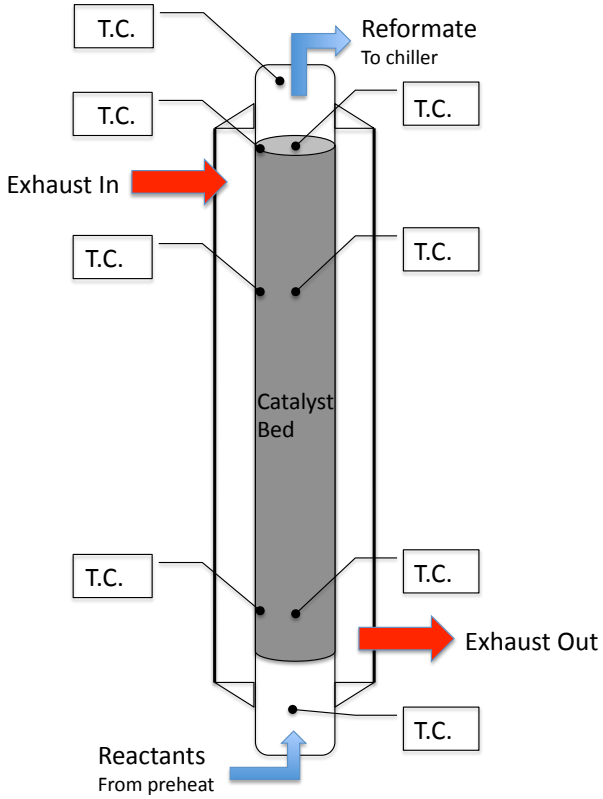


Figure 3.6: Steam Reformer Schematic

in place with heavy stainless steel mesh discs on either end. Catalyst bed temperature measurement was done with an array of six K type stainless steel jacketed thermocouples inserted in through the top, and was done at three axial locations. The thermocouples were positioned at each axial location at the reactor wall and on the centerline, and were held in place with stainless steel mesh. These thermocouples were positioned at axial locations 40mm (1.6”), 330mm (13”), and 600mm (23.6”) from the bottom of the catalyst bed.

#### 3.2.1.1 Bed Size

The steam reformer bed length of 60cm was determined with the help of a quasi-1D numerical model. Using results from [12, 13, 35] a numerical model of the steam reformer incorporating heat transfer, mass transfer, and chemical kinetics was constructed in MAT-

Figure 3.7: Catalyst Pellets

LAB. This model was then compared to experimental data from other steam reformers in the lab to validate it, and was found to be in good agreement. Using measured fuel consumption rates for the engine used and measured exhaust gas temperatures, a reactor bed length was designed to ensure that high fuel conversion would occur over a range of space velocities.

### 3.2.2 Heat Exchanger

The heat exchanger of the reactor is a double pipe design, with the inner tube the reactor and the outer shell holding the exhaust from the engine. It is a closed heat exchanger design; the exhaust flow and reactant flow do not mix. The reactants can be directed to enter either end of the reactor tube, allowing for either counterflow or coflow heat exchanger operation with respect to exhaust flow. The exhaust is routed to the heat exchanger through a 50mm (2") diameter SS304 exhaust line and is isolated from engine vibrations with a flex coupling. The exhaust line is heavily insulated with a ceramic refractory fiber, and protected from impact, abrasion, and general wear with a gypsum bonded fiberglass. The outside of the heat exchanger is heavily insulated with a high temperature ceramic fiber, designed for refractory use. This delicate fiber was held in place and protected from abrasion with fiberglass cloth. Temperature measurements of the exhaust gas are taken at the inlet and outlet of the heat exchanger via thermocouples inserted into the center of the exhaust stream.

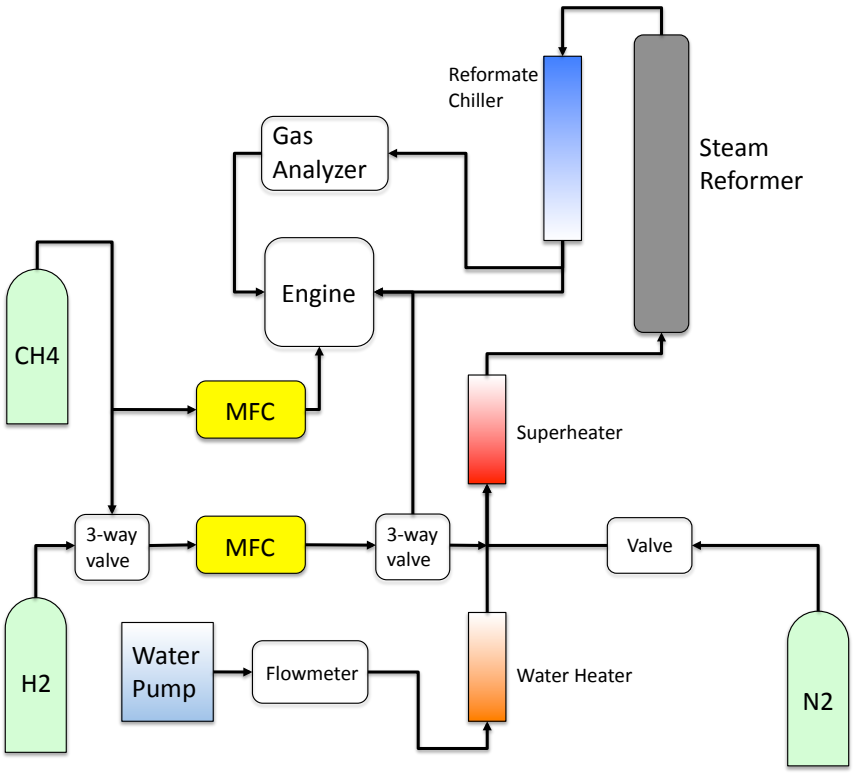


Figure 3.8: Fuel Delivery Schematic

## 3.3 Fuel Delivery System

Fuel is routed through a pressure regulator from the high pressure supply, and regulated to 69kPa (10 psi). The fuel is divided through two Mass Flow Controllers (MFCs), one measuring virgin fuel to the engine, the other controlling gas flow to the steam reformer. An $N_2$ supply is connected with a shut off valve to the steam reformer supply line, to provide a purge while the system is not in use and for use in decoking the reactor bed. The gas is then mixed with steam and heated to inlet temperatures in the preheat system, then directed with a three way valve to the top or bottom of the reactor. At the reactor outlet the gas is cooled and the condensate is removed prior to deliver to the engine or analysis. A schematic of the flow system is shown in Figure 3.8.

### 3.3.1 Water System

The water is pumped and measured by a metering gear pump and ultrasonic liquid flowmeter. The flow rate is controlled using a PI controller to maintain a flow set point. The water is drawn from a tank that is pressurized to the inlet pressure of the preheat system, which minimizes the disturbance input with flow rate set point changes through the reactor.

#### 3.3.1.1 Flowrate Measurement

The flow rate of water in the system is measured with an Atrato Ultrasonic liquid flowmeter. This low pressure drop, low flow rate liquid measurement device has specifications as shown in Table 3.2 and is well suited to accurate measurement of flow rates less than 1L/min. It has a user definable measurement range and output voltage.


Figure 3.9: Atrato ultrasonic liquid flowmeter

Table 3.2: Atrato ultrasonic liquid flowmeter specifications

| | |
|---|---|
| Flow Range | 2mL/min - 20L/min |
| Linearity | ±1.5% over flow range |
| Repeatability | ±0.5% |
| 0-5V output | ±0.1% linearity |

#### 3.3.1.2 Pump

To supply water to the system a gear pump from Cole-Parmer is used. It is controlled via a voltage signal to vary the pressure of the water to achieve a desired flow rate. It has interchangeable heads for different water flow rates, and can develop a maximum pressure of about 345kPa (50 psi).

### 3.3.2 Gas System

The gas system is composed of gas flow measurement and control, pressure regulators, and a reformate cooler and dryer. The gas is fed from a tank of 2.0 grade (certified 99% chemical purity) Methane, supplied by Praxair. It is regulated down to 345kPa (50 psi) at the first shut off valve, then fed to the steam reformer gas flow control and to the engine through the secondary regulator.

#### 3.3.2.1 Mass Flow Controllers

To measure and control the flow of gas, several mass flow controllers made by Omega Engineering were used (Figure 3.10). Each has an error associated with the full range so they were chosen so that the typical flow rate would be between 40 and 80 percent of the rated flow. One mass flow controller (MFC) was used to measure the flow of virgin fuel to the engine. It was operated in meter only mode and was not used to control the flow of gas. The secondary MFC was used to control the flow of gas to either the steam reformer or to the engine for co-fueling tests. The MFCs have internal, normally closed solenoids which prevent gas flow in the event of a loss of power.


Figure 3.10: Mass Flow Controller

Table 3.3: Mass Flow Controllers

| Rated Flow Rate (SLPM) | Error (% of full range) | Function |
|---|---|---|
| 100 | 2.0 | engine fuel measurement |
| 50 | 2.0 | reactor fuel control |

#### 3.3.2.2 Reformate Chiller and Dryer

At the exit of the steam reformer the reformate stream is at an elevated temperature, in excess of 400°C, and it must be cooled before it is drawn into the engine. As well, there is a significant amount of water vapor in the reformate stream that must be removed. This is accomplished through a series of double pipe heat exchangers fed with 25°C water from the building plumbing and a water trap to catch entrained droplets. The resulting stream is directed to analysis or to the engine. A schematic is shown in Figure 3.11.

### 3.3.3 Preheat System

The reactants must be heated prior to their introduction to the steam reformer. This is done in multiple stages. First the water is pumped through a copper tube coiled in the exhaust line, downstream of the reactor heat exchanger. The water vapor then flows through some heater subassemblies, consisting of stainless steel pipe fittings and cartridge heaters amounting to 2,400W of electrical heating power. The cartridge heaters were controlled using phase control modules to vary the power output. The power draw was measured using a self powered inductive ammeter which has a measurement range of 0-100A and delivers a 0-5V signal. A schematic is shown in Figure 3.12.

### 3.3.4 Control System

All reactant flow, heaters, engine load, and other parameters, as well as measurement and data collection was done using a custom LabView code. USB devices from Phidgets were used to collect thermocouple readings and engine speed. An Arduino Mega was used to generate analog voltage signals, read analog inputs, and set digital states to control mass flow controllers, phase control modules, and the water pump. A schematic is shown in Figure 3.13.

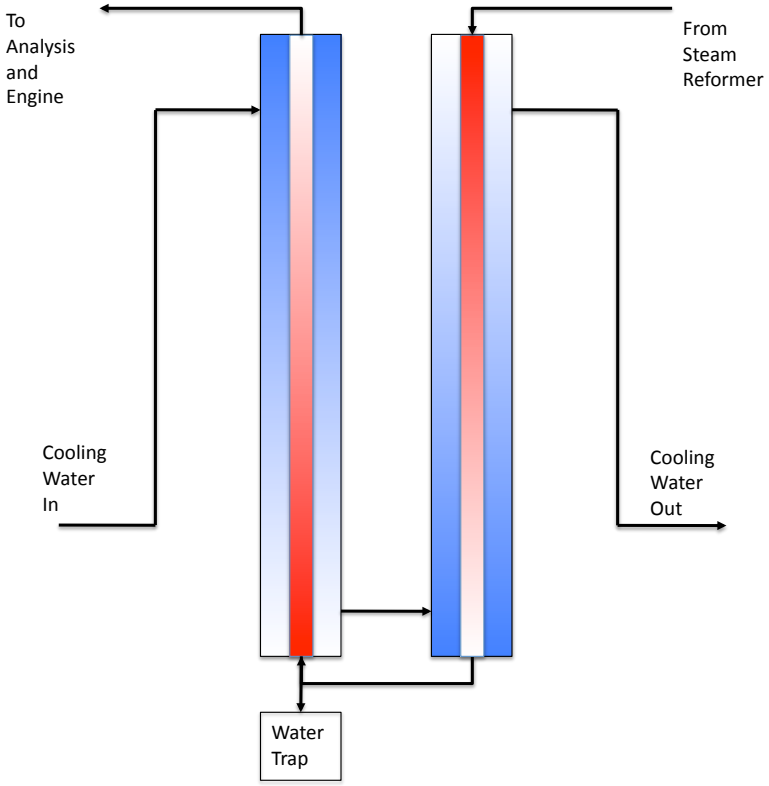


Figure 3.11: Reformate Chiller Schematic

### 3.3.5 Gas Analysis

Analysis of reformer effluent was done with a NOVA Analytics gas analyzer, capable of detecting molar percentages of $H_2$, $CH_4$, $CO$, and $CO_2$. It has calibrated detection limits, over which the voltage signal will be saturated. These limits were set to be in the normal range for steam reforming products.

## 3.4 Experimental Procedure

Experiments were taken over a period of five months in varying conditions. The system was operated in the Hydrogen Production and Utilization Lab (HyPAUL) at University of California, Davis, which maintained a relatively stable temperature over changing seasons. First, engine tests with bottled gas were completed to establish baseline operation at dif-

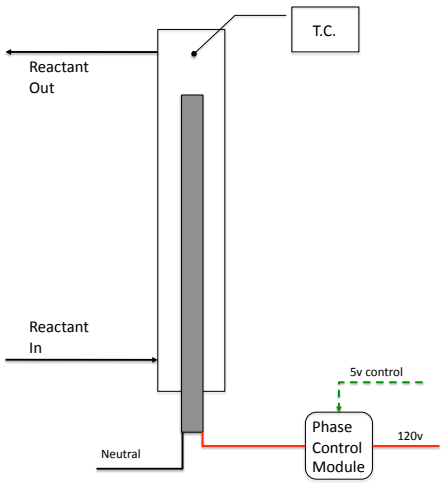


Figure 3.12: Preheat Schematic (single heater)

ferent compositions of $H_2$ and $CH_4$, as well as to determine maximum brake torque spark timing and the lean stability limit as a function of composition. Steam reformer tests were done to establish operational range, and closed loop tests were completed to investigate the effect of engine stoichiometry and steam reformer load on system performance.

### 3.4.1 Start Up

Inexpensive commercial odorized propane was used for engine and reactor warm up. All shut off valves were verified to be in the off position, where they were left while the system was not in use for safety. The main fuel regulator was then set for propane, at 3kPa (12" W.C.) as specified by the manufacturer for propane. Lambda adjustment through fuel needle valve was set for richer mixture for start. The ignition system was turned on, and timing advance set to be $< 30°$. Connection to the control computer was verified. The brake load was verified to be disconnected. The propane fuel tank was then opened, and ll shut off valves were opened. The engine was started and run in a no load condition under mechanical governor control for 2 minutes. The brake load was then connected, and the brake load control system was allowed to take over from mechanical governor at a set throttle position (WOT). The engine was run until catalyst bed temperatures were stable, typically 15-20 minutes. The brake load was disconnected and the engine

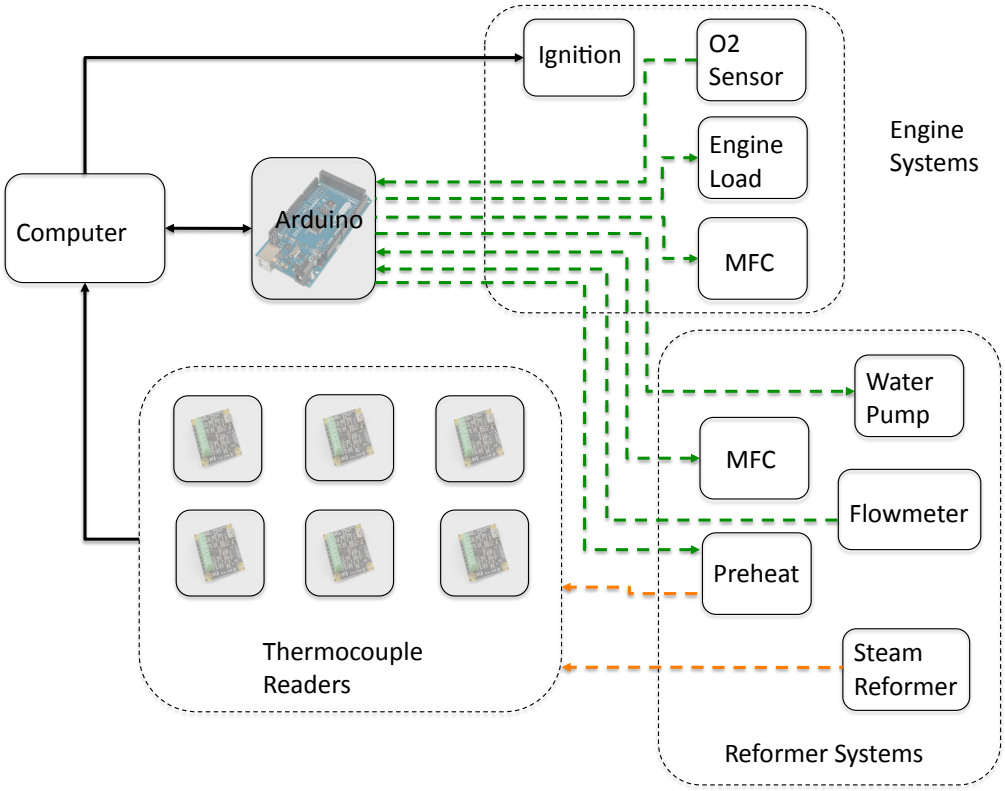


Figure 3.13: Control Schematic

was allowed to run for 1 minute in a no load condition under mechanical governor control before shut down. The warmup fuel tank and all shut off valves were then closed, and the main fuel regulator was adjusted for operation with methane, to 1.5kPa (6" W.C). The fuel supply was then opened.

### 3.4.2 Operation

Operation proceeded in a similar way to start up. With the main fuel regulator set for operation with methane, and all shut off valves opened, the engine could be started up in a no load condition under control of the mechanical governor. After 2 minutes the brake load was engaged, and experiments could proceed.

#### 3.4.2.1 Engine Experiments

Engine experiments were conducted to determine MBT spark timing for the test engine at different percentages of $H_2$ and different stoichiometries at WOT. This is essential in any investigation involving different compositions as the change in flame speed can significantly change the optimal timing for a particular $\lambda$. These tests were all completed at a set engine speed and throttle position, 3600 RPM and WOT, respectively. The engine was run on a mixture of bottled methane and hydrogen in different volumetric percentages and at different stoichiometries as described above. The set points are shown in Table 3.4. The spark timing was varied at each fuel composition and $\lambda$ set point and the thermal efficiency $\eta_{TH,indicated}$ was measured. MBT spark timing could then be determined from the maximum thermal efficiency at each composition and stoichiometry tested.

Table 3.4: Open Loop Engine Test Settings

| Factor | Low level | Mid level | High level |
|---|---|---|---|
| $\lambda$ | 1.0 | 1.5 | LSL |
| $\%H_2$ | 0.0% | 10% | 50% |

#### 3.4.2.2 Reformer Experiments

Steam reformer experiments were done by running the engine on propane at a set power level and varying the exhaust temperature through adjustments in $\lambda$, examining the effect on the conversion, yield, and efficiency of the steam reformer. These tests were done to determine reactor performance based on bed temperature and flow rate. The steam reformer set points are shown below in Table 3.5. First the steam reformer bed temperatures were allowed to stabilize. The water flow was initiated at the desired flow rate based on the set $S/C$ ratio, and the preheat system enabled. Methane flow was also begun at the desired set point, and both water and gas were directed through the reactor bypass until the inlet temperature set point was reached by the preheat system. The reactant mixture was then diverted through the steam reformer and maintained at a steady level until the reformate composition and reactor bed temperatures had stabilized.

Table 3.5: Open Loop Steam Reformer Test Settings

| Factor | Low level | High level |
|---|---|---|
| EGT | 700°C | 800°C |
| Flowrate | 5 SLPM | 15 SLPM |

#### 3.4.2.3 Closed Loop Thermochemical Recuperation Experiments

The engine was examined in conjunction with the TCR unit, to determine the performance of the system based on engine stoichiometry $\lambda$ and steam reformer load. The engine was run without any flow through the steam reformer as describe above. The reactant flow was then initiated at a low level, and directed through the reactor bypass until the preheat system had stabilized the reactant inlet temperature, at which point the reactant flow was diverted through the steam reformer. Reactant flow rates and engine stoichiometry were slowly adjusted to reach the desired set points, which are shown below in Table 3.6. Ignition timing was adjusted based on fuel composition and $\lambda$ to reference timing as determined from the open loop engine experiments utilizing bottled gas.

Table 3.6: Closed Loop Thermochemical Recuperation Test Settings

| Factor | Low level | Mid level | High level |
|---|---|---|---|
| $\lambda$ | 1.0 | 1.5 | LSL |
| % Fuel Reformed | 0 | 25 | 50 |

### 3.4.3 Possible Faults and their detection

There are a number of faults that can occur that must be avoided for stable operation. These faults can be detected both through direct observation, as well as observed in the final data, through the use of the standard error. These faults were avoided in the final presented data, and repeatability of these experiments was verified. The faults and methods of their detection are described in detail below.

#### 3.4.3.1 Engine Faults

The engine can suffer from several faults that result in unreliable data. The ignition timing can be too advanced or retarded for a given stoichiometry or fuel composition;

this can cause misfire. Similarly excessively lean mixtures can cause misfire; these are both detectable audibly. Excessively advanced ignition in the presence of hydrogen is hazardous, as the flame front can advance upstream through the intake and ignite the air filter. This was detected audibly as a loud popping explosion and visibly from the flames that developed. Care was taken not to advance the spark timing excessively in the presence of hydrogen. High temperature and excessive vibration has an extremely deleterious effect on the structural integrity of the exhaust system. On several occasions this caused fractures and eventual breakage of the exhaust line, shown below in Figure 3.14. This was remediated by replacement of all mild steel parts with stainless steel.

Figure 3.14: Two examples of exhaust line failure

#### 3.4.3.2 Reactor Faults

Reactor faults were primarily related to the inadvertent production of coke. In the event of a low water flow condition a very low $S/C$ ratio existed until water flow was restored; this promoted the formation of solid carbon deposits in the steam reformer. The amount of coke developed did not approach levels detectable in the output composition; the activation of the catalyst bed was not significantly affected. However, the solid carbon had a tendency to become lodged downstream of the reactor in restrictions, causing a high pressure drop through the reactor and severely limiting flow through the system. Shown in Figure 3.15 are some examples of the coking on the catalyst pellets and in the tubes downstream of the reactor.

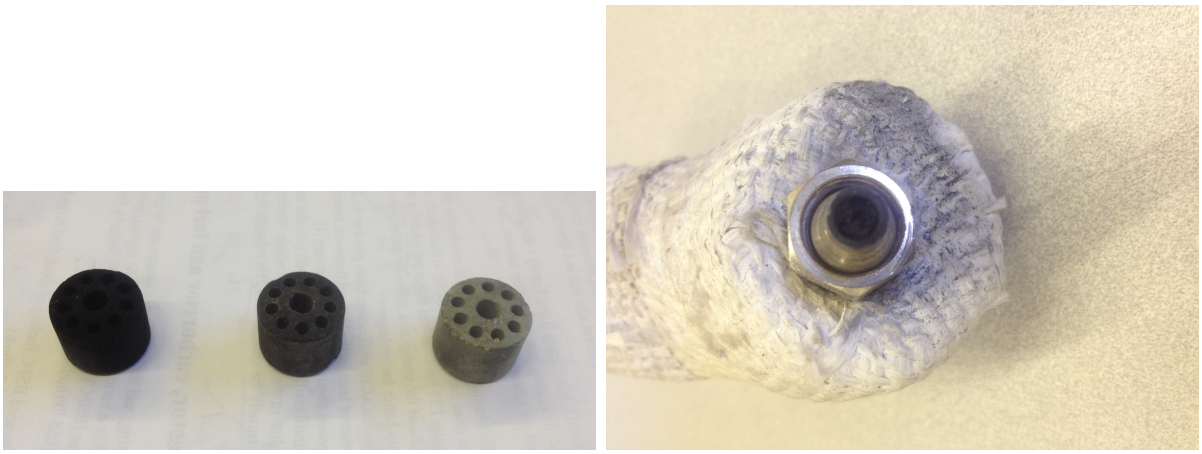

Figure 3.15: Coking on catalyst pellets in various stages (L) and carbon deposits downstream of steam reformer (R)

## 3.5 Factorial Design

To determine the effects of multiple factors, a factorial experimental design was employed. A $2^2$ matrix is used to examine the effects and interactions of $\lambda$ and the steam reformer load as a fraction of total fuel flow on the system efficiency $\eta_{sys}$. The resulting model can be a reasonable predictor of the output given the input factors in the range in which the system was examined.

### 3.5.1 Independent and Dependent Variables

Critical to the design of a good factorial experiment is the selection of appropriate variables for analysis. The independent variables selected were the air fuel equivalence ratio $\lambda$ and the steam reformer load, as a percentage of total fuel flow. Levels for these factors were selected based on early investigations utilizing the experimental apparatus, and are presented in Table 3.7.

Table 3.7: Factors and corresponding levels

| Factors (inputs) | Low Level (-) | High Level (+) |
|---|---|---|
| $X_1$ ($\lambda$) | 1.0 | 1.5 |
| $X_2$ (% reformed) | 0% | 25% |

The most relevant dependent variable for this study is the brake thermal efficiency of

the system, $\eta_{sys}$, as defined in 2.31. The test configurations are shown in Table 3.8

Table 3.8: Experimental design matrix

| Run (experiment configuration) | $X_1$ $\lambda$ | $X_2$ %reformed | Degrees of freedom |
|---|---|---|---|
| 1 | - | - | 3 |
| 2 | - | + | 3 |
| 3 | + | - | 3 |
| 4 | + | + | 3 |

### 3.5.2 Randomization

To avoid hysteresis issues due to engine wear, catalyst degradation, and other unaccounted for variables, efforts were made to randomize the run order of the various set points. Shown below in Table 3.9 is the actual run order used for the factorial experiments. This does not represent every experiment performed, only the order of experiments included in the factorial model.

Table 3.9: Factorial Experiment Run Order

| Run (experiment configuration) | Run Order |
|---|---|
| 1 | 1,3,6,9 |
| 2 | 8,10,15,16 |
| 3 | 2,4,5,14 |
| 4 | 7,11,12,13 |

### 3.5.3 Statistical Analysis

Analysis was done on the data collected for the factorial experiments to determine a model incorporating effects and interactions of both independent variables. The variance of each individual run was calculated as shown in Equation 3.1.

$$S_i^2 = \frac{\sum_j^r (Y_j - \bar{Y})^2}{r-1} \tag{3.1}$$

$\bar{Y}$ is the average output for a run configuration and $r$ is the number of repetitions performed. The pooled standard deviation for all experiments $S_p$ was calculated from the individual variances $S_i$, as shown in Equation 3.2:

$$S_p = \sqrt{\frac{\sum_i^n S_i^2}{n}} \tag{3.2}$$

where $n$ is the total number of experimental configurations. The standard error, used for evaluating the statistical significance of the effects and interactions, is calculated as in Equation 3.3:

$$S_E = \frac{2 \cdot S_p}{\sqrt{n_f}} \tag{3.3}$$

where $n_f$ is the total number of all experiments performed including replication. The effects and interactions are calculated as shown in Equations 3.4 and 3.5.

$$E_i = \frac{\sum_{run=1}^{4} X_{i,run} \cdot \bar{Y}_{run}}{2} \tag{3.4}$$

$$I_{i,j} = \frac{\sum_{run=1}^{4} X_{i,run} \cdot X_{j,run} \cdot \bar{Y}_{run}}{2} \tag{3.5}$$

where $X_{i,run}$ is +1 for the high level setting and -1 for the low level setting. A model for a $2^2$ factorial experiment can be constructed from these effects and interactions $E_i$ and $I_{i,j}$ as shown in Equation 3.6.

$$Y = \bar{Y} + \frac{E_1}{2}X_1 + \frac{E_2}{2}X_2 + \frac{I_{1,2}}{2}X_1X_2 \tag{3.6}$$

The statistical significance of these effects $E_i$ and interactions $I_{i,j}$ can be determined by comparing the signal to noise ratio $t$-ratio as calculated in Equation 3.7 to the critical $t$-ratio at the desired confidence interval for the experiment's total degrees of freedom. The effect is considered statistically significant if the absolute value of the $t$-ratio is greater than the critical value.

$$t* = \frac{E \text{ or } I}{S_E} \tag{3.7}$$

# Chapter 4

# Results and Discussion

## 4.1 Open Loop

The systems were first examined in a piecewise capacity. Information about the engine and steam reformer was needed in order to determine appropriate operating points for the closed loop test. The engine was examined in terms of the stoichiometry with different fuel compositions, with the engine set at reference timing. The stability limit was determined for different settings.

### 4.1.1 Engine Results

The performance of the engine was first examined using bottled gases to determine MBT spark timing at different $\lambda$ values and compositions, which was used later in the operation of the closed loop system. Three important outputs, the brake thermal efficiency $\eta_{TH}$, the power output, and the exhaust gas temperature are examined below in terms of the inputs.

#### 4.1.1.1 Efficiency

The brake thermal efficiency was measured for the purpose of characterizing the engine and determining MBT spark timing. The results of this open loop testing are shown below in Figure 4.1.

As can be seen from this best fit surface, there were minor effects on $\eta_{TH}$ with respect to the addition of $H_2$, at lower values of $\lambda$, above the stoichiometric case. However, $\eta_{TH}$ is much more dependent on $\lambda$, with a moderately higher values between $\lambda$ values of 1

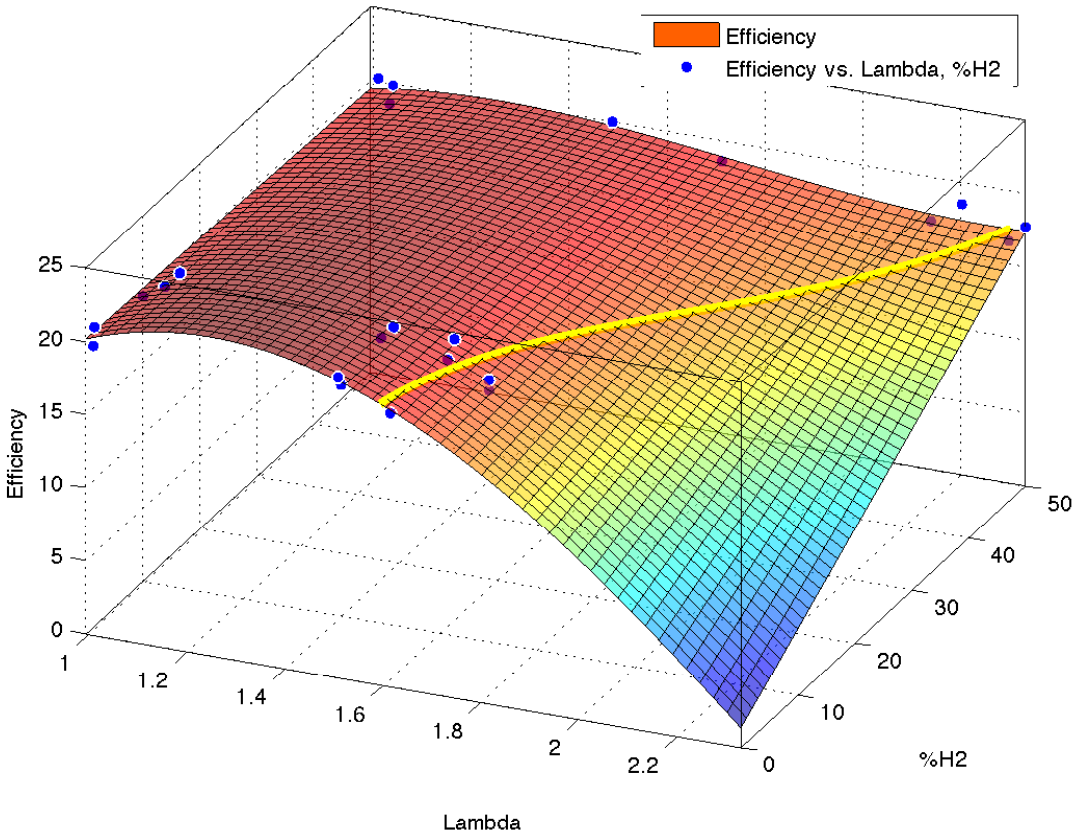


Figure 4.1: Open Loop Engine Brake Efficiency at 3600 RPM, as a function of $\lambda$ and $\%H_2$ in the fuel stream. The surface line denotes the lean stability limit.

and 1.5 and lower values beyond that. The sharpness of the decrease in $\eta_{TH}$ is strongly dependent on the composition, with greater percentages of $H_2$ significantly increasing the efficiency at higher values of $\lambda$. Shown on the surface in Figure 4.1 is a line denoting the lean limit as determined by these open loop experiments as a function of $\%H_2$ in the fuel stream. This was used as a guide for closed loop operation for determination of lean operating conditions.

#### 4.1.1.2 Power

Power output of the engine was measured, and mapped with respect to $\lambda$ and composition. The results are shown below in Figure 4.2.

This map, as described by the best fit polynomial surface, shows a slight decrease in the power output with increasing $H_2$ in the fuel stream. This is to be expected as there

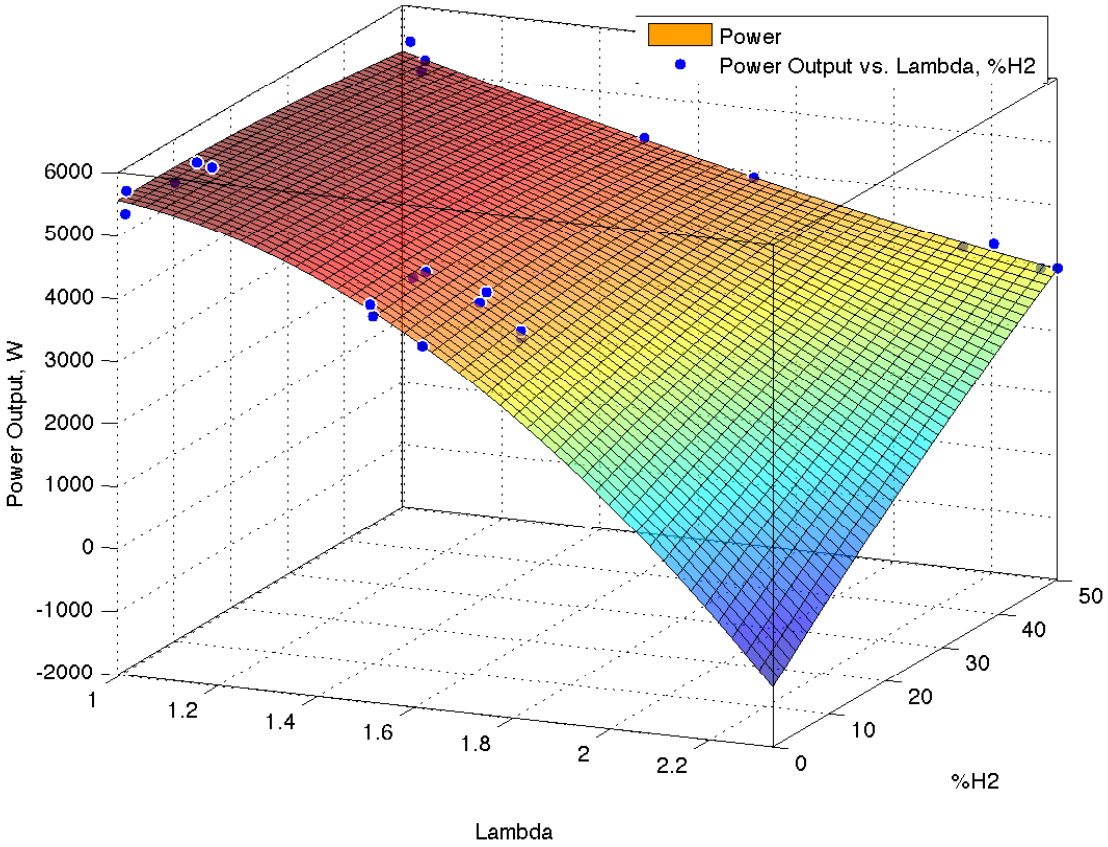


Figure 4.2: Open Loop Engine Power at 3600 RPM

is reduced energy density in gaseous $H_2$ with respect to $CH_4$. As well, this map shows a nearly linear decrease in power with increasing values of $\lambda$ at higher percentages of $H_2$ in the fuel stream, but a rapid decrease beyond $\lambda$ values of about 1.6 with no $H_2$ in the fuel stream.

#### 4.1.1.3 Exhaust temperature

Exhaust temperature was measured, as excessive temperatures can have a negative effect on engine wear and lifetime, but higher temperatures offer greater potential for recovery. The exhaust gas temperature was mapped by $\lambda$ and volumetric percentage $H_2$ in the fuel stream, and is shown below in Figure 4.3.

This best fit surface of exhaust gas temperatures shows some obvious trends. As can be expected, as the engine charge becomes leaner there is a decrease in the exhaust gas temperature. There are minimal effects of the composition on the exhaust gas tempera-

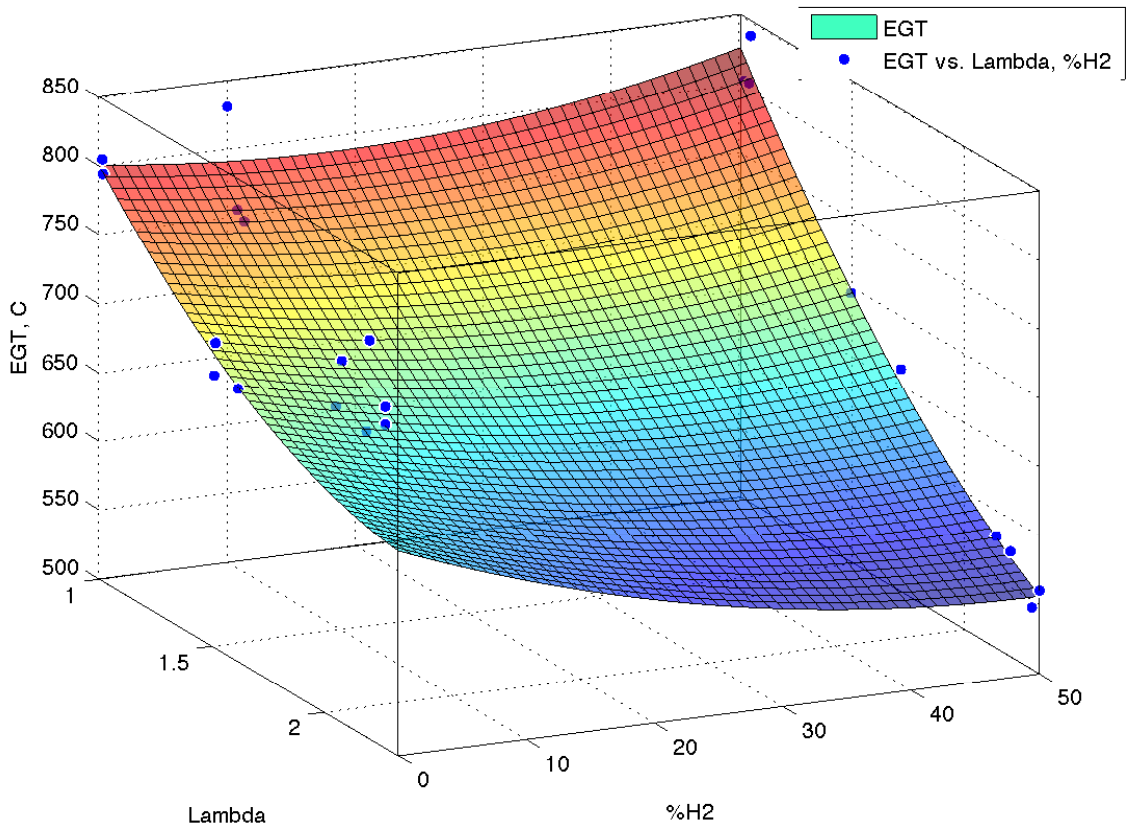


Figure 4.3: Open Loop Engine Exhaust Gas Temperature at 3600 RPM

ture.

#### 4.1.1.4 Stability Limit

One of the most apparent effects of $H_2$ addition was the extension of the lean stability limit. This is clearly seen in Figures 4.1 and 4.2, which shows a break point where the surface dramatically changes slope. Figure 4.2 showed a nearly linear decrease in output power at high percentages $H_2$ for the range of $\lambda$ explored, while at lower percentage $H_2$ compositions the decrease in power is roughly linear, but decreases rapidly due to misfire, partial burn, and other abnormal combustion events. These were audibly apparent during testing.

Similarly, in Figure 4.1, it can be seen that depending on the percentage of $H_2$ in the fuel stream, that within a range of $\lambda$ there are only small changes to $\eta_{TH}$, and at $\lambda$ values greater than this range $\eta_{TH}$ decreases rapidly. This rapid decrease can be attributed to the

abnormal combustion events, which were audibly apparent during testing. The extension of the stability limit can be attributed to the addition of $H_2$, and the corresponding reduction of these abnormal combustion events at a given value of $\lambda$. This was denoted by the solid line as shown in Figure 4.1.

#### 4.1.1.5 Summary

The effect of $H_2$ addition on engine performance was limited for a number of important metrics, including brake thermal efficiency $\eta_{TH}$ and output power, but still discernible. The greatest effect was on the allowable range of operation for $\lambda$, in which there was a significant extension of stable operation to much leaner regimes.

### 4.1.2 Steam Reformer Results

The steam reformer component was examined as a component to determine its performance at different bed temperatures and flow rates. The performance was measured in several ways, including conversion $X_{CH_4}$, percent yield $H_2$ $Y_{H_2}$, and efficiency $\eta$. The results are displayed below as best fit surfaces.

#### 4.1.2.1 Conversion

Conversion, an important reactor parameter, was mapped by reactor bed temperature and $CH_4$ molar flow rate. The ratio $S/C$ was fixed at 3 to prevent coking. The results are shown below in Figure 4.4.

As can be seen from this figure, at the flow rates used there is a strong temperature dependence on conversion, as well as a weak dependence on reactant flow rate. A higher average bed temperature shows a general increase in conversion, as can be expected of a steam reformer. The low conversion at both low and high flow rates and low temperatures can likely be attributed to a kinetic limitation.

#### 4.1.2.2 Yield

Yield is more appropriate when the reactor is used for processing hydrocarbons for fuel cells or to produce $H_2$ for chemical processes other than combustion. Figure 4.5 below shows the effect of average reactor bed temperature and molar flow rate, mapped to a best fit polynomial surface.

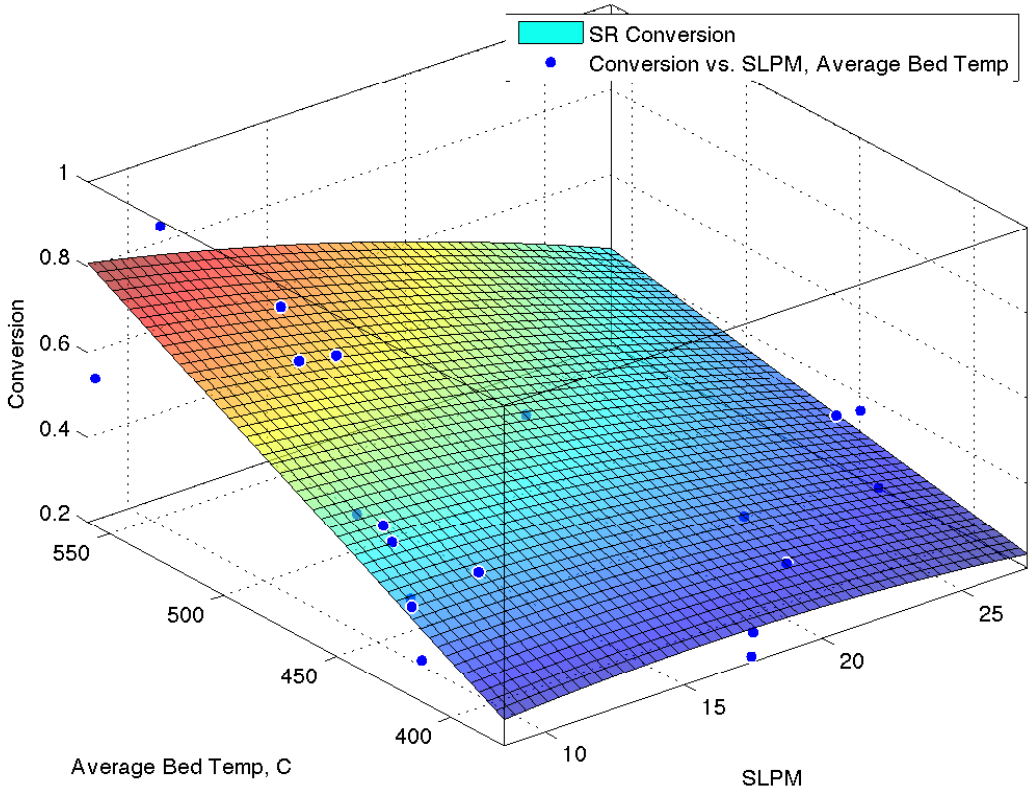


Figure 4.4: $CH_4$ Conversion by Flow Rate and Bed Temperature

The best fit polynomial surface suggests that in this operational range suggests that there is a dependence both on flow rate and mean catalyst bed temperature, but a stronger dependence on temperature. High yields at high temperatures and low flow rates is expected, as neither the heat transfer nor the mass transfer limitations are significant.

#### 4.1.2.3 Efficiency

For the purposes of recovering thermal energy for use in combustion processes, thermal efficiency can be described as in Equation 2.7, in which the primary concern is the change of the heating value of the fuel. As the heat of reaction is supplied from a waste source, this can be considered appropriate. Note that this definition does not account for the sensible energy in the reformate stream, which is not recovered. As shown in Figure 4.6 below, $\eta$ is shown as a function of mean reactor bed temperature and molar flow rate $CH_4$.

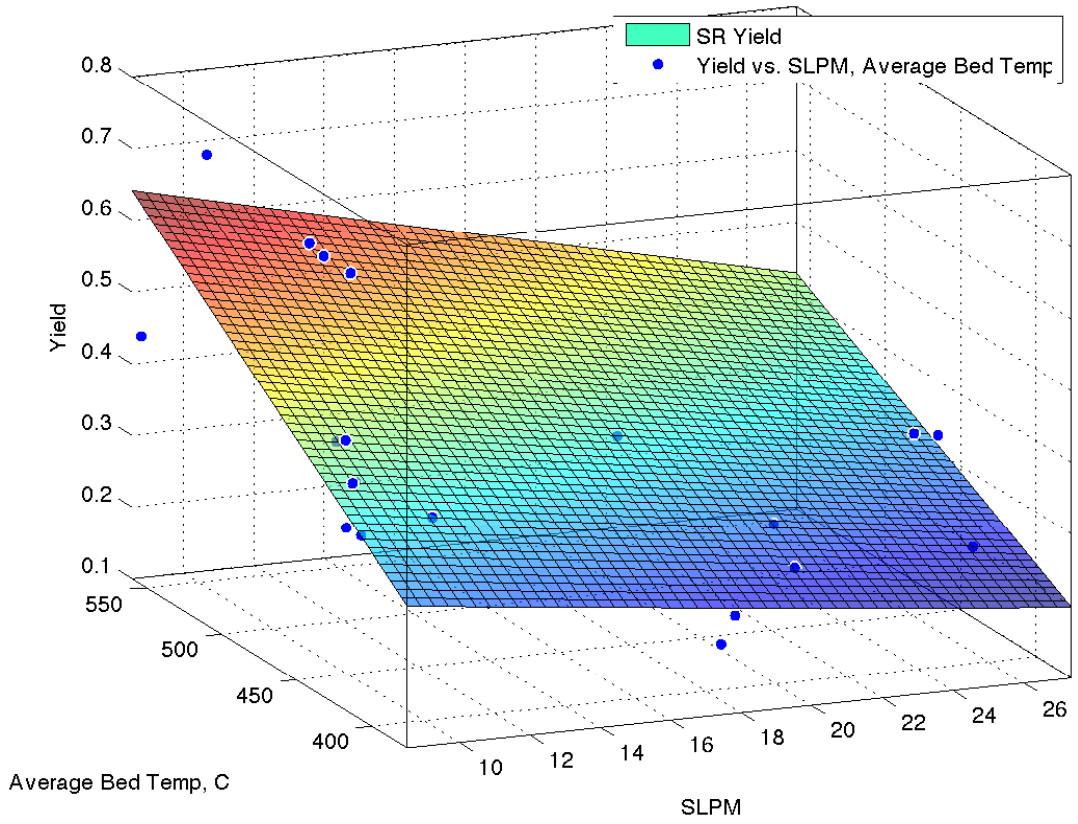


Figure 4.5: Yield $Y_{H_2}$ of Steam Reformer

As is seen here, the effect of reactant flow rate had a small effect on efficiency. Temperature played the dominant role on the steam reformer efficiency $\eta$. This is intuitive as the steam reforming reactions are highly endothermic, and the greater the thermal resource the greater the chemical recovery potential.

#### 4.1.2.4 Summary

The performance of the steam reformer can be described by the above surface maps. This data can give some insight into appropriate operating points for the closed loop system, such as flow rates. The fact that there appears to be only a slight dependance on flow rate for all reactor metrics suggests that the steam reformer is heat transfer limited rather than mass transfer limited - a diffusional limitation would likely manifest as a decrease in the performance at a given temperature, as seen above around 450°C in the above Figures 4.4, 4.5, and 4.6 at higher flow rates.

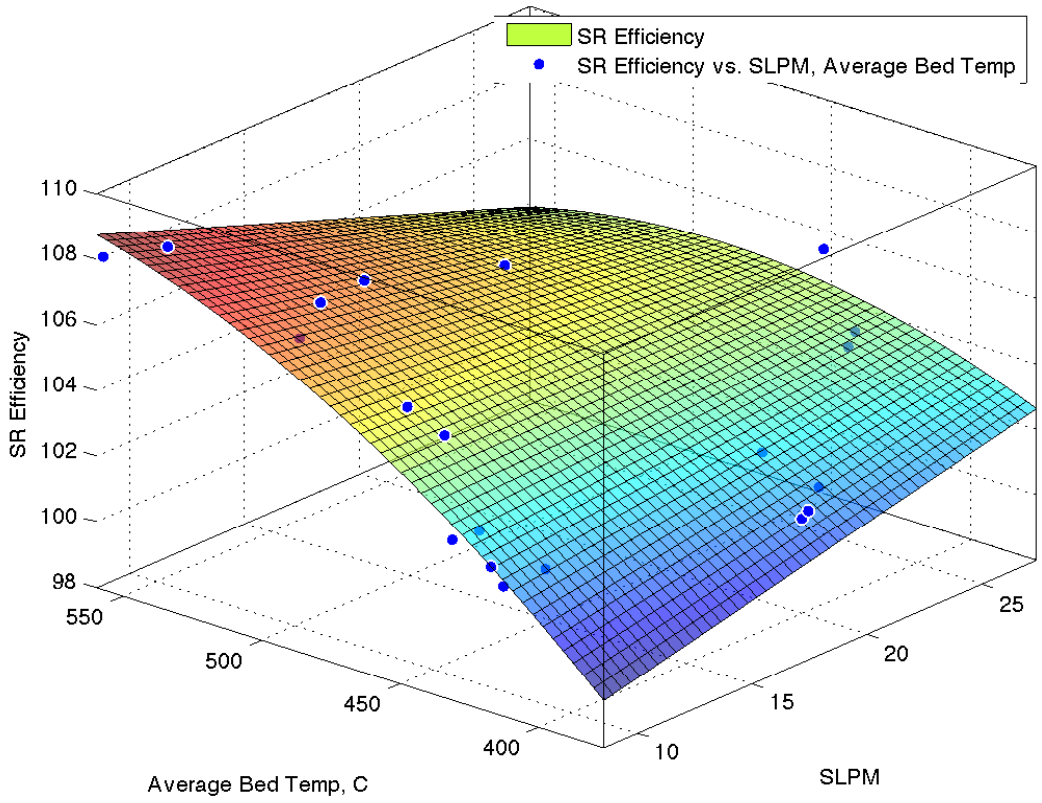


Figure 4.6: Efficiency of Steam Reformer based on $LHV$ of reformate stream

## 4.2 Closed Loop

The operation of the closed loop system was examined in terms of system efficiency, exhaust temperature, and power output at WOT operation at 3600 RPM. The results are shown below.

### 4.2.1 Efficiency

System efficiency $\eta_{sys}$ was mapped in terms of $\lambda$ and both the percentage of virgin fuel diverted through the steam reformer and the percentage of $H_2$ in the fuel stream from the steam reformer.

As can be seen from Figures 4.7 and 4.8, there is generally a poorer fit for these surfaces to the data versus the open loop engine tests. When $\eta$ is examined as a function of the percentage $H_2$ (Figure 4.8) there is a negative relationship between $\lambda$ and system

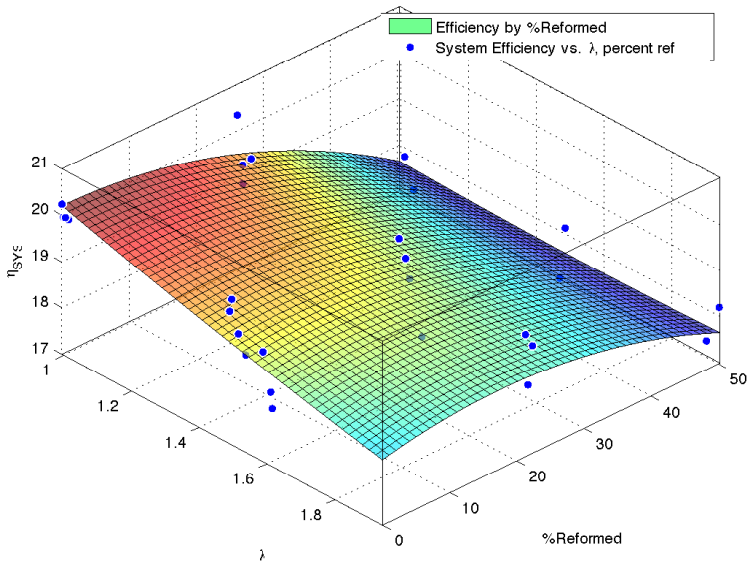


Figure 4.7: $\eta_{SYS}$ vs. % fuel stream reformed by volume

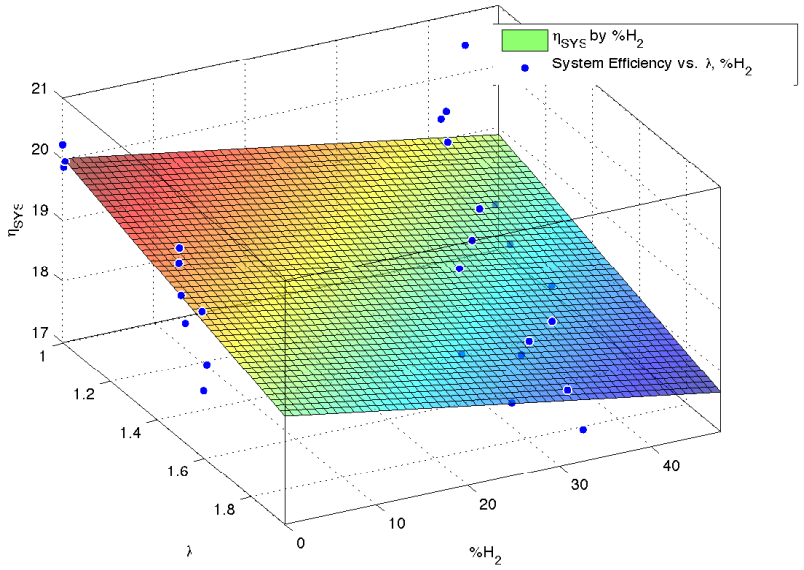


Figure 4.8: $\eta_{SYS}$ vs. % $H_2$ in fuel stream

efficiency $\eta_{sys}$, and a negative relationship between $\%H_2$ and $\eta_{sys}$. Taken in contrast to Figure 4.1 these two figures show similar trends, though the lean stability limit is not well identified from the data presented in Figure 4.8. When $\eta_{sys}$ is examined as a function of the percentage of fuel diverted to the steam reformer (Figure 4.7) the trends are similar,

showing negative effects on $\eta_{sys}$ from both.

#### 4.2.1.1 Factorial Analysis

A factorial analysis was completed on the effect of air fuel equivalence ratio $\lambda$ and the percentage of fuel diverted to the steam reformer on system efficiency $\eta_{sys}$. The experimental set points as described in Table 3.7 were evaluated and the results are presented below in Table 4.1.

Table 4.1: Summary of factorial experiments

| Run | $X_1$ $\lambda$ | $X_2$ %reformed | $\eta_{sys}$ | $\bar{\eta}_{sys}$ | $S^2$ |
|---|---|---|---|---|---|
| 1 | - | - | 19.87, 20.24, 19.98, 19.99 | 20.02 | 0.0240 |
| 2 | - | + | 19.49, 19.66, 20.62, 19.10 | 19.72 | 0.4164 |
| 3 | + | - | 18.96, 19.36, 19.87, 20.12 | 19.58 | 0.2705 |
| 4 | + | + | 19.72, 19.25, 18.91, 17.47 | 18.84 | 0.9459 |

It can be seen that the magnitude of $S^2$ is greater for the high levels of both factors. The statistical analysis of the factorial experiment is presented in Table 4.2.

Table 4.2: Statistical analysis of factorial experiment results

| Overall efficiency $\eta_{sys}$ | $S_p$ | $S_E$ | Total degrees of freedom |
|---|---|---|---|
| 19.54 | 0.3716 | 0.1858 | 12 |

The effects and interactions can be computed as in Equations 3.4 and 3.5 from the data presented in Tables 4.1 and 4.2. These effects are shown in Table 4.3 below.

Table 4.3: Effects and interactions of the input variables

| | |
|---|---|
| Effect of $\lambda$ ($E_1$) | -0.6593567064 |
| Effect of steam reformer load ($E_2$) | -0.520971579 |
| Interaction of $\lambda$ and steam reformer load ($I_{1,2}$) | -0.22018634 |

The effects and interaction are negative for all factors. These can be used to construct a model as shown in Equation 3.6, which can be used as a predictor of system efficiency $\eta_{sys}$

in the range explored. However the statistical significance of these effects and interaction must be evaluated. The results are presented in Table 4.4.

Table 4.4: Signal-to-noise $t$-ratio and statistical significance

| | $t*$ | Significant at 95% confidence? | Significant at 99% confidence? |
|---|---|---|---|
| Student $t$-value at 95% confidence | 2.179 | - | - |
| Student $t$-value at 99% confidence | 3.055 | - | - |
| Effect of $\lambda$ ($E_1$) | -3.549 | Yes | Yes |
| Effect of steam reformer load ($E_2$) | -2.804 | Yes | No |
| Interaction of $\lambda$ and steam reformer load ($I_{1,2}$) | -1.185 | No | No |

As can be seen only the effects of $\lambda$ and steam reformer load are statistically significant at the 95% confidence level. At the 99% confidence level only the effect of $\lambda$ is significant.

### 4.2.2 Power

Power was measured and is displayed here with best fit surfaces. As can be seen in Figures 4.9 and 4.10, there is a decrease in output power at WOT with increasing steam reformer load and % $H_2$ in the fuel stream. This is consistent with the results found in open loop operation with bottled gas.

The lower energy density of the fuel stream on a volumetric basis yields a slightly lower power output at the same air fuel equivalence ratio $\lambda$ with increasing steam reformer load.

### 4.2.3 Exhaust Temperature

Exhaust Temperature EGT was measured and is displayed with a best fit surface. As shown in Figures 4.11 and 4.12 the effect is dominated by $\lambda$, and there is only a small contribution from the effect of the steam reformer and % $H_2$ in the fuel stream.

As discussed earlier, $NO_x$ production is proportional to temperature, and exhaust gas temperature can be used as a rough indicator of peak temperatures in the absence of in cylinder measurement. As EGT is proportional to $\lambda$ the trend for $NO_x$ production is

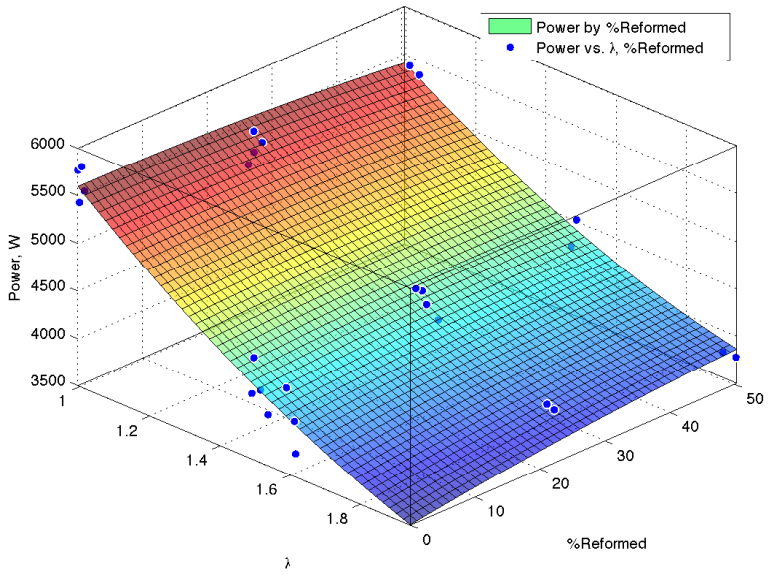


Figure 4.9: Power vs. $\lambda$, % fuel stream reformed by volume

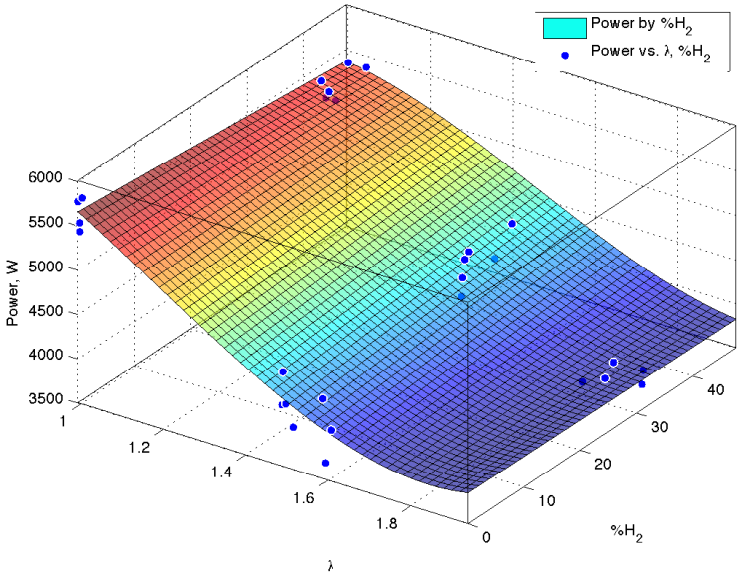


Figure 4.10: Power vs. $\lambda$, % $H_2$ in fuel stream

expected to follow $\lambda$, though as shown earlier higher in cylinder temperatures for greater proportions of $H_2$ in the fuel stream means that there are higher levels of $NO_x$ at a given $\lambda$ with more $H_2$ enrichment.

Seen in Figure 4.13 is the tailpipe temperature $\text{EGT}_{out}$, the exhaust temperature

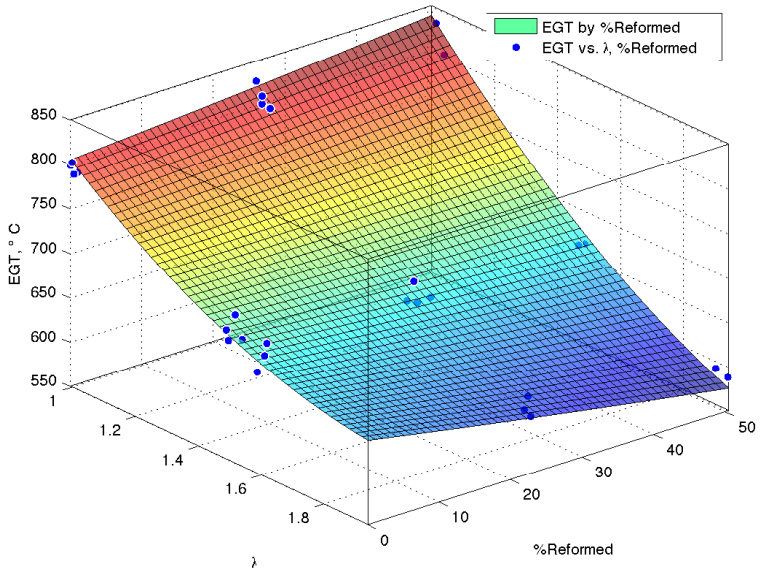


Figure 4.11: EGT vs. $\lambda$, % fuel stream reformed by volume

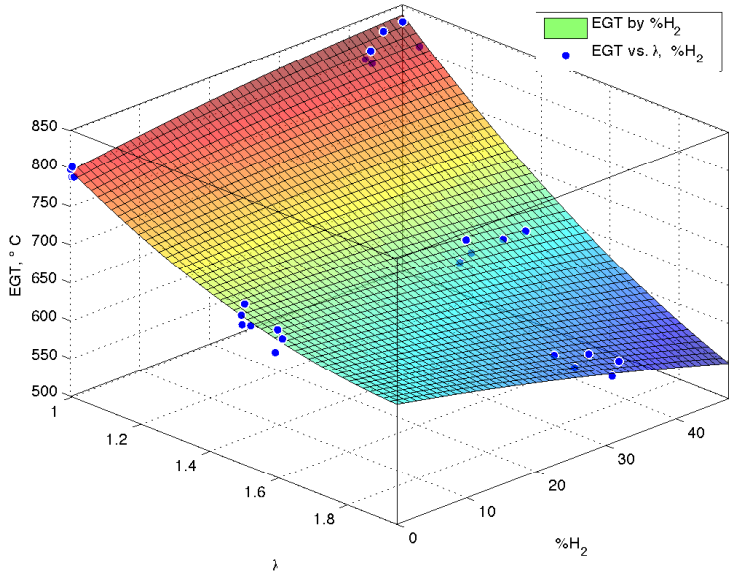


Figure 4.12: EGT vs. $\lambda$, % $H_2$ by volume in fuel stream

downstream of the steam reformer. It is plotted against $\lambda$ and steam reformer reactant flow rate. As can be expected, there is a negative relationship between $\lambda$ and $\mathrm{EGT}_{out}$, just as there is a strong dependence between EGT and $\lambda$. There is also a negative relationship between reactant flow rate and $\mathrm{EGT}_{out}$, which shows that greater reactant

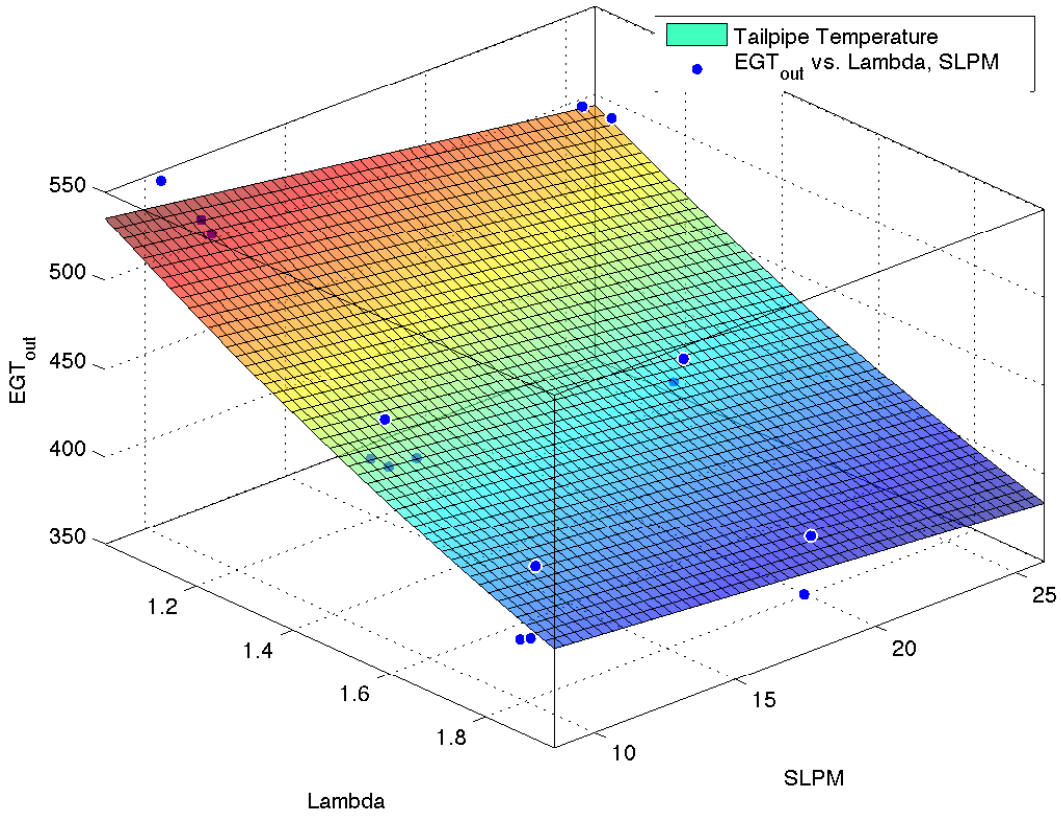


Figure 4.13: Tailpipe Exhaust Temperature $\mathrm{EGT}_{out}$ vs. Reactant Flow Rate and $\lambda$

flow rate increases the heat recovery from the exhaust stream. Figure 4.13 clearly shows that there is still a significant thermal resource available.

### 4.2.4 Stability Limit

The extension of the lean stability limit was examined as a function of the percentage of $H_2$ in the fuel stream, as determined from the open loop engine experiments done with bottled gas. The lean stability limit was determined based on these open loop experiments, and engine stoichiometry $\lambda$ was set based on the measured $H_2$ in the fuel stream from the steam reformer.

### 4.2.5 Exhaust Heat Recovery

The performance of the heat exchanger used to transfer heat from the exhaust to the steam reformer was measured by looking at the change in temperature of the exhaust

gas and the enthalpy change across the steam reformer. This included sensible energy in the reformate stream. The heat into the steam reformer $Q_{in}$ and the heat loss to the environment $Q_{loss}$ can then be determined.

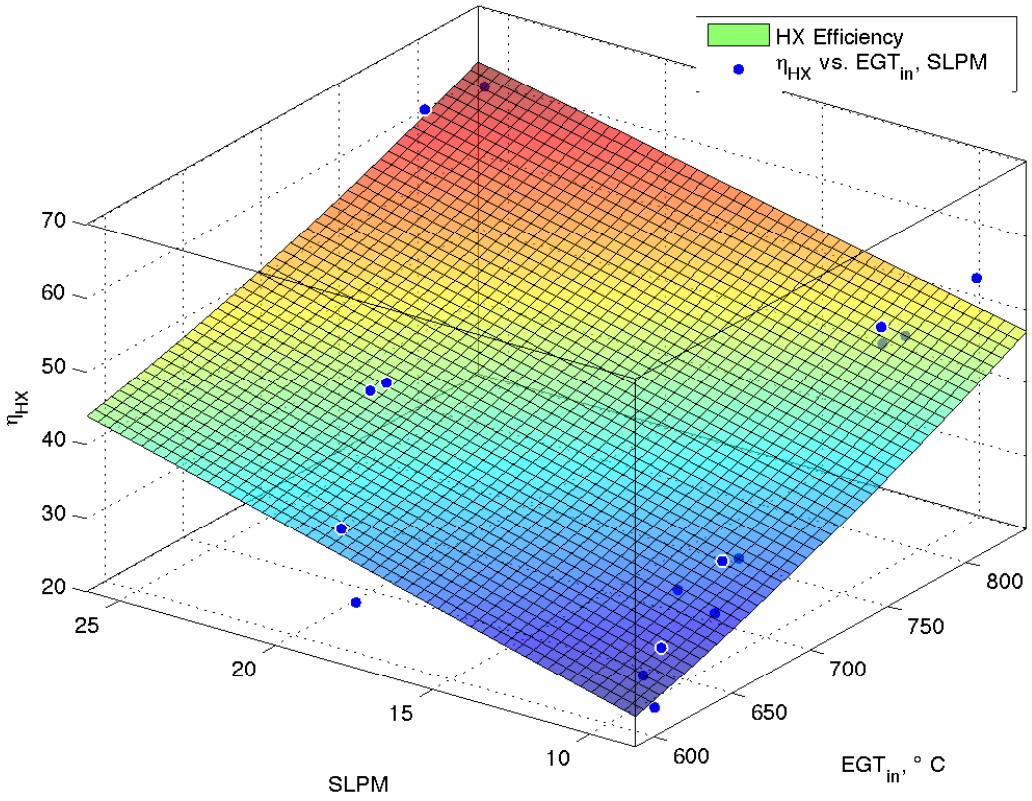


Figure 4.14: Heat Exchanger Efficiency vs. EGT & Reactant Flow Rate

Figure 4.14 shows a positive relationship between EGT and heat exchanger efficiency $\eta_{HX}$. This is intuitive as higher exhaust temperatures mean a greater thermal gradient. The steam reforming process is highly temperature dependent, and higher conversion further increases this thermal gradient. As well, there is a positive relationship between reactant flow rate and $\eta_{HX}$. Greater reactant flow rate increases the convective heat transfer from the reactor wall to the reactants.

The losses of the heat exchanger can also be mapped as a function of EGT and reactant flow rate. This is shown in Figure 4.15. This similarly shows that there is a negative relationship between EGT and losses; greater exhaust temperatures create a

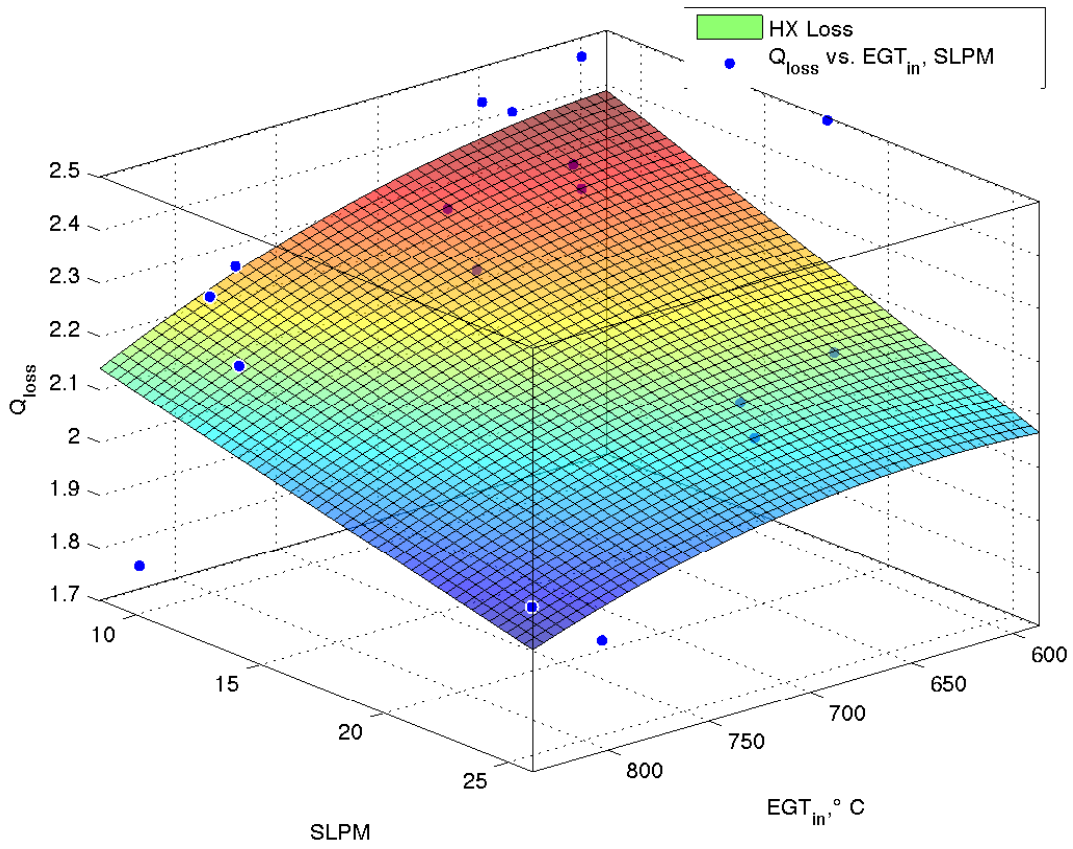


Figure 4.15: Heat Exchanger Loss vs. EGT & Reactant Flow Rate

greater thermal gradient, reducing losses. As well, higher reactant flow rates improve convective heat transfer from the reactor wall, reducing losses to the environment. Low flow rates and low EGT contributed to higher heat exchanger losses. Figure 4.15 shows that there are significant thermal resources that are lost to the environment that are not recovered at all; there is room for improvement in the heat exchanger design to improve thermal recovery.

### 4.2.6 Other Characteristics

#### 4.2.6.1 Fuel Composition

The performance of the steam reformer can be mapped with respect to air fuel equivalence ratio $\lambda$ and the percentage diverted to the steam reformer. The percentage of $H_2$ in the fuel stream as a function of these two is shown in Figure 4.16.

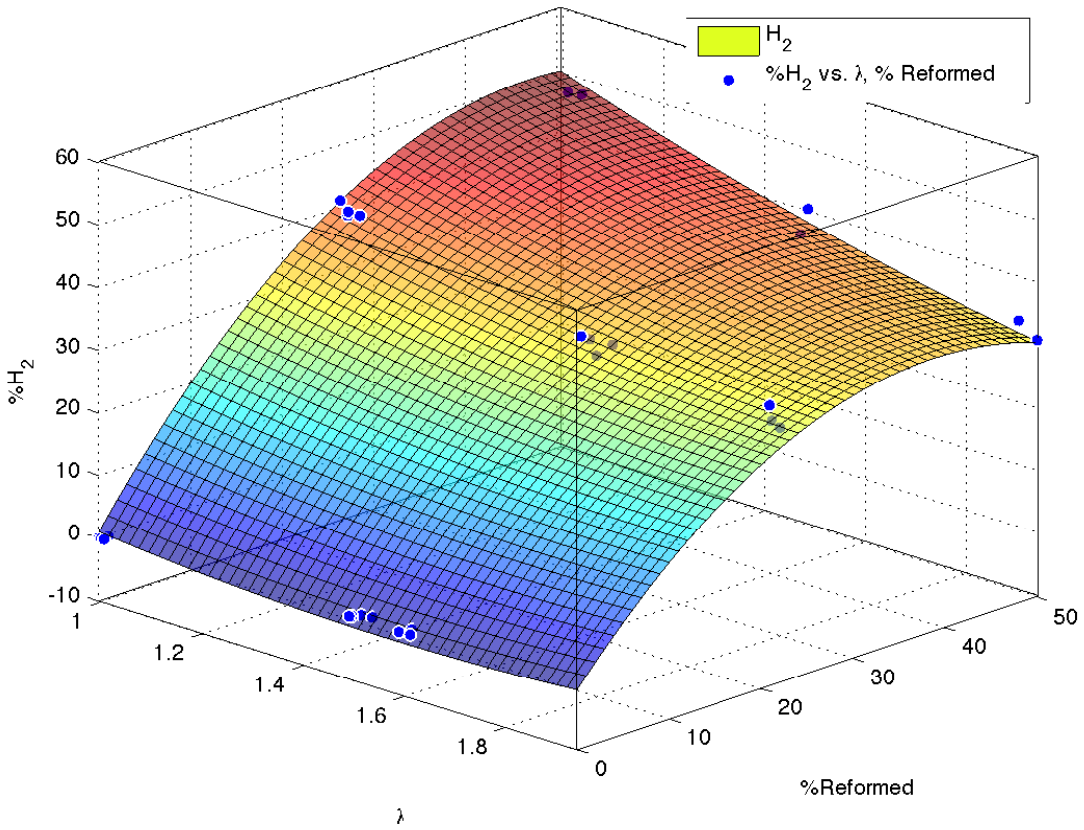


Figure 4.16: Percentage $H_2$ by volume in Fuel Stream

As can be seen there is a strong dependence for the amount of $H_2$ in the fuel stream on the amount of fuel reformed, as can be expected. Similarly there is a negative relationship between $\lambda$ and $H_2$ production, which can be explained by the temperature dependence of $H_2$ production.

#### 4.2.6.2 Parasitic Load

The parasitic load, which was excluded in the energy accounting used for efficiency calculations, is none the less an important characteristic for system performance. A best fit surface is shown in Figure 4.17.

As can be seen, there is a strong relationship between reactant flow rate and parasitic load, mostly reflecting the heating load of the water. Greater EGT has a negative effect on the parasitic load, due to the heating provided by the exhaust on the preheat system. This parasitic loading could be reduced by further thermal recovery from the engine exhaust.

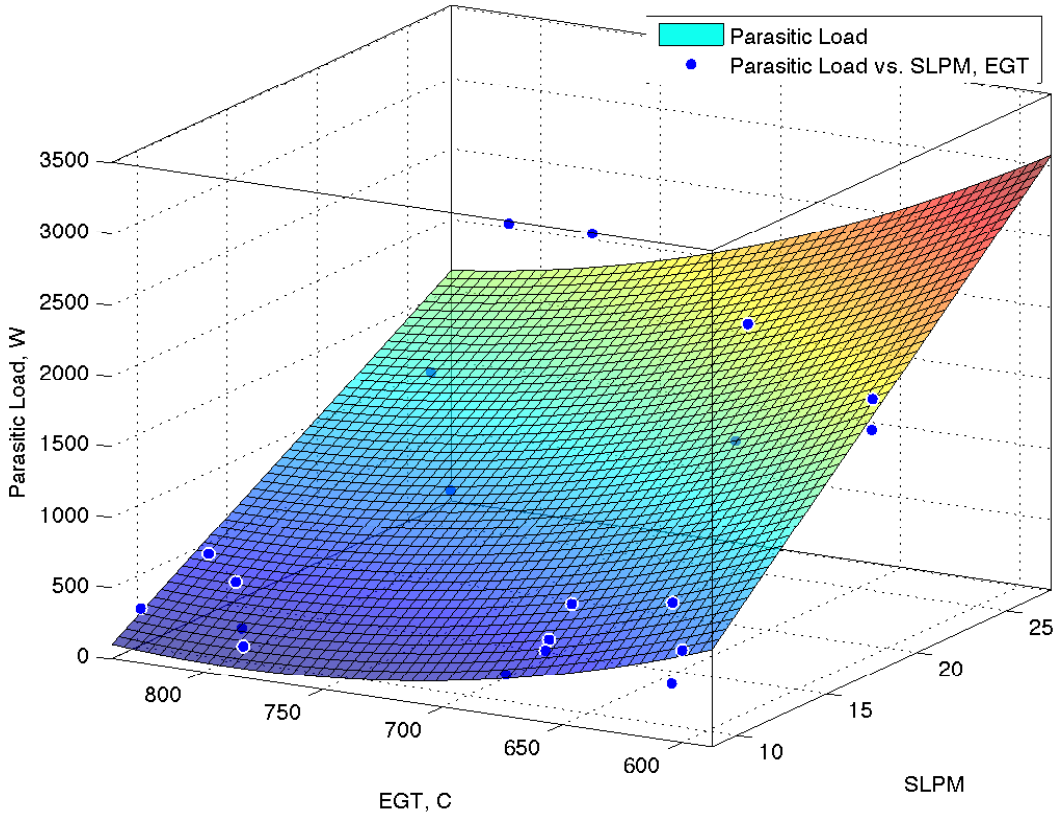


Figure 4.17: Parasitic load vs. EGT & Reactant Flow Rate

As well, the parasitic loading could be reduced by thermal recovery of the hot reformate stream; this sensible energy is currently rejected.

### 4.2.7 Summary

Closed loop operation of a thermochemical recuperating system was successfully demonstrated. Overall there is a negative relationship between both $\lambda$ and steam reformer load, for system efficiency $\eta_{sys}$. This represents a worst case scenario, as there is still significant room for improvement in terms of steam reformer design and thermal recovery, both from engine exhaust and from the hot reformate stream. An extension of the lean limit was demonstrated, and the engine was run at much lower power levels at WOT through the use of the TCR system. The percentage of $H_2$ in the fuel stream is nearly linear up to the level tested, as the yield is quite high. Though at higher levels of steam reformer load

there is increasing heat exchanger efficiency, the steam reformer seems to be limited by thermal considerations as conversion drops at the same bed temperature and the heat is recovered as sensible enthalpy rather than chemical potential.

# Chapter 5

# Conclusions and Recommendations

This project demonstrated that it is possible to run a single cylinder spark ignition engine on methane, utilizing a TCR unit to provide hydrogen as a portion of the fuel stream. As well, it was demonstrated that this system could allow much leaner charge mixtures, resulting in an extension of the lean limit and a greater operational range without the use of throttling. There were no identified gains in overall system efficiency due to the use of the TCR system, despite the exhaust heat recovery; however it was also recognized that this represents a worst case scenario, as heat exchanger efficiencies were less than 50% in most cases, and sensible energy from the hot reactant stream was not recovered.

## 5.1 Recommendations for Future Work

This work could be extended in a number of possible ways. A number of experiments can be performed with the existing experimental apparatus, including further investigation into the performance of the system at different input levels. Though every effort was made to set the ignition spark timing appropriately, a variable output composition from the TCR system made optimal spark timing difficult, which likely impacted results.

### 5.1.1 Equipment Modifications

The experimental apparatus utilized in these experiments could be modified to further explore the potential of TCR. As was indicated previously, there are relatively low heat exchanger efficiencies in the TCR system, which limits the potential heat recovery especially

when considered on the basis of recovered chemical potential rather than the production of hydrogen for the extension of the lean limit. This could be done by exploring the aspect ratio of the steam reformer and heat exchanger to improve heat transfer characteristics. Preheat of reactants was largely done electrically for convenience, but greater heat recovery is possible to preheat reactants prior to entry into the steam reformer. Other chemical reactors could be explored, perhaps utilizing different catalyst structures or chemistries. As EGT is significantly lower in lean operating conditions, other reactors with better performance at low temperatures could be utilized. As the experiments performed by the author indicated that the greatest performance gain from the utilization of the TCR system was in the extension of the lean limit and not in energy recovery, thermo-neutral or possibly exothermic reactors could be used to produce hydrogen.

### 5.1.2 Research Topics

The extension of the lean limit through the use of TCR opens up the possibility of improving the overall efficiency of a spark ignition engine utilized in a variable drive cycle. Given that there is some data based on the steady state performance of this experimental apparatus utilizing TCR, data could be put in simulations to estimate improvements based on this and other work. All experiments were conducted at steady state, and as transient thermal effects, which are ever-present in real systems, can be significant on highly endothermic processes, work in this area can be done.

# References


[1] John B Heywood. *Internal combustion engine fundamentals*, volume 930. Mcgraw-hill New York, 1988.

[2] S Orhan Akansu, Zafer Dulger, Nafiz Kahraman, and T Nejat Veziroğlu. Internal combustion engines fueled by natural gas—hydrogen mixtures. *International Journal of Hydrogen Energy*, 29(14):1527–1539, 2004.

[3] Zhongquan Gao, Xiaomin Wu, Hui Gao, Bing Liu, Jie Wang, Xiangwen Meng, and Zuohua Huang. Investigation on characteristics of ionization current in a spark-ignition engine fueled with natural gas–hydrogen blends with bss de-noising method. *international journal of hydrogen energy*, 35(23):12918–12929, 2010.

[4] David R Vernon, Eddie A Jordan, Jonathon M Woolley, and Paul A Erickson. The potential for exhaust heat recovery by thermochemical recuperation for hydrogen enriched internal combustion. In *ASME 2007 Internal Combustion Engine Division Fall Technical Conference*, pages 705–713. American Society of Mechanical Engineers, 2007.

[5] R Saidur, M Rezaei, WK Muzammil, MH Hassan, S Paria, and M Hasanuzzaman. Technologies to recover exhaust heat from internal combustion engines. *Renewable and Sustainable Energy Reviews*, 16(8):5649–5659, 2012.

[6] Toshio Shudo, Yosuke Shima, and Tatsuya Fujii. Production of dimethyl ether and hydrogen by methanol reforming for an hcci engine system with waste heat recovery–continuous control of fuel ignitability and utilization of exhaust gas heat. *International Journal of Hydrogen Energy*, 34(18):7638–7647, 2009.

[7] A Tsolakis and A Megaritis. Partially premixed charge compression ignition engine with on-board h2 production by exhaust gas fuel reforming of diesel and biodiesel. *International Journal of Hydrogen Energy*, 30(7):731–745, 2005.

[8] Y Jamal and ML Wyszynski. On-board generation of hydrogen-rich gaseous fuels—a review. *International Journal of Hydrogen Energy*, 19(7):557–572, 1994.

[9] D Yap, SM Peucheret, A Megaritis, ML Wyszynski, and H Xu. Natural gas hcci engine operation with exhaust gas fuel reforming. *International Journal of Hydrogen Energy*, 31(5):587–595, 2006.

[10] A Tsolakis, A Megaritis, and ML Wyszynski. Low temperature exhaust gas fuel reforming of diesel fuel. *Fuel*, 83(13):1837–1845, 2004.

[11] Andrew E. Lutz, Robert W. Bradshaw, Jay O. Keller, and Dennis E. Witmer. Thermodynamic analysis of hydrogen production by steam reforming. *International Journal of Hydrogen Energy*, 2003.

[12] Kaihu Hou and Ronald Hughes. The kinetics of methane steam reforming over a ni/$\alpha$-al¡ sub¿ 2¡/sub¿ o catalyst. *Chemical Engineering Journal*, 82(1):311–328, 2001.

[13] Jianguo Xu and Gilbert F Froment. Methane steam reforming, methanation and water-gas shift: I. intrinsic kinetics. *AIChE Journal*, 35(1):88–96, 1989.

[14] DL Trimm. Coke formation and minimisation during steam reforming reactions. *Catalysis Today*, 37(3):233–238, 1997.

[15] Hyung Chul Yoon, Jonathan Otero, and Paul A Erickson. Reactor design limitations for the steam reforming of methanol. *Applied Catalysis B: Environmental*, 75(3): 264–271, 2007.

[16] David D Davieau and Paul A Erickson. The effect of geometry on reactor performance in the steam-reformation process. *International journal of hydrogen energy*, 32(9): 1192–1200, 2007.

[17] C. Liao and Paul A. Erickson. Characteristic time as a descriptive parameter in steam reformation hydrogen production processes. *International Journal of Hydrogen Energy*, 2008.

[18] Hyung Chul Yoon. *Comparison of Steam and Autothermal Reforming of Methanol for Fuel Cell Applications*. PhD thesis, University of California, Davis, 2008.

[19] David Dennis Davieau. *An analysis of space velocity and aspect ratio parameters in steam-reforming hydrogen production reactors*. PhD thesis, University of California, Davis, 2004.

[20] Paul A Erickson and Chang-hsien Liao. Statistical validation and an empirical model of hydrogen production enhancement found by utilizing passive flow disturbance in the steam-reformation process. *Experimental Thermal and Fluid Science*, 32(2):467–474, 2007.

[21] Paul A Erickson. Statistical validation and an empirical model of hydrogen production enhancement found by utilizing a controlled acoustic field in the steam-reforming process. *International journal of hydrogen energy*, 31(12):1690–1697, 2006.

[22] Chi-Hsiung Li and BA Finlayson. Heat transfer in packed bedsa reevaluation. *Chemical Engineering Science*, 32(9):1055–1066, 1977.

[23] H Scott Fogler. *Elements of chemical reaction engineering*. Prentice-Hall International London, 1999.

[24] Subir Roychoudhury, Marco Castaldi, Maxim Lyubovsky, Rene LaPierre, and Shabbir Ahmed. Microlith catalytic reactors for reforming *iso*-octane-based fuels into hydrogen. *Journal of power sources*, 152:75–86, 2005.

[25] R Byron Bird, Warren E Stewart, and Edwin N Lightfoot. *Transport phenomena*. John Wiley & Sons, 2007.

[26] Jens R Rostrup-Nielsen. Production of synthesis gas. *Catalysis today*, 18(4):305–324, 1993.

[27] Jens Sehested. Four challenges for nickel steam-reforming catalysts. *Catalysis Today*, 111(1):103–110, 2006.

[28] D. L. Trimm. Catalysts for the control of coking during steam reforming. *Catalysis Today*, 1999.

[29] DL Trimm. Control of coking. *Chemical Engineering and Processing: Process Intensification*, 18(3):137–148, 1984.

[30] BR Stanmore, JF Brilhac, and P Gilot. The oxidation of soot: a review of experiments, mechanisms and models. *Carbon*, 39(15):2247–2268, 2001.

[31] Martin Skov Skjøth-Rasmussen. Modelling of soot formation in autothermal reforming. *Technical University of Denmark*, 2003.

[32] N Müller, A Jess, and R Moos. Direct detection of coke deposits on fixed bed catalysts by electrical sensors. *Sensors and Actuators B: Chemical*, 144(2):437–442, 2010.

[33] Norbert Müller, Sebastian Reiß, Peter Fremerey, Andreas Jess, and Ralf Moos. Initial tests to detect quantitatively the coke loading of reforming catalysts by a contactless microwave method. *Chemical Engineering and Processing: Process Intensification*, 50(8):729–731, 2011.

[34] Gerhard Fischerauer, Martin Förster, and Ralf Moos. Sensing the soot load in automotive diesel particulate filters by microwave methods. *Measurement Science and Technology*, 21(3):035108, 2010.

[35] Joonguen Park, Shinku Lee, Sungkwang Lim, and Joongmyeon Bae. Heat flux analysis of a cylindrical steam reformer by a modified nusselt number. *International Journal of Hydrogen Energy*, 34(4):1828–1834, 2009.

[36] Juliana Piña and Daniel O Borio. Modeling and simulation of an autothermal reformer. *Latin American Applied Research J*, 36:289–294, 2006.

[37] RL Hoekstra, K Collier, N Mulligan, and L Chew. Experimental study of a clean burning vehicle fuel. *International Journal of Hydrogen Energy*, 20(9):737–745, 1995.

[38] P Erickson, D Vernon, Eddie Jordan, Kirk Collier, and Neal Mulligan. Low nox operation and recuperation of thermal and chemical energy through hydrogen in internal combustion engines. In *Proceedings of the 16th Annual Hydrogen Conference of the National Hydrogen Association (NHA) April*, 2005.

[39] Kirk Collier, Robert L Hoekstra, Neal Mulligan, Charles Jones, and Douglas Hahn. Untreated exhaust emissions of a hydrogen-enriched cng production engine conversion. Technical report, SAE Technical Paper, 1996.

[40] BE Milton and JC Keck. Laminar burning velocities in stoichiometric hydrogen and hydrogen hydrocarbon gas mixtures. *Combustion and Flame*, 58(1):13–22, 1984.

[41] Fabien Halter, Christian Chauveau, and Iskender Gökalp. Characterization of the effects of hydrogen addition in premixed methane/air flames. *International Journal of Hydrogen Energy*, 32(13):2585–2592, 2007.

[42] RW Schefer. Hydrogen enrichment for improved lean flame stability. *International Journal of Hydrogen Energy*, 28(10):1131–1141, 2003.

[43] G Yu, CK Law, and CK Wu. Laminar flame speeds of hydrocarbon+ air mixtures with hydrogen addition. *Combustion and Flame*, 63(3):339–347, 1986.

[44] David R. Vernon. *Hydrogen Enrichment and Thermochemical Recuperation in Internal Combustion Engines: An Investigation of Dilution and Inlet Temperature Effects in the Autothermal Reformation of Ethanol.* PhD thesis, University of California, Davis, 2010.

[45] P Van Blarigan and JO Keller. A hydrogen fuelled internal combustion engine designed for single speed/power operation. *International Journal of Hydrogen Energy*, 23(7):603–609, 1998.

[46] Juan Li, Zhenwei Zhao, Andrei Kazakov, and Frederick L Dryer. An updated comprehensive kinetic model of hydrogen combustion. *International Journal of Chemical Kinetics*, 36(10):566–575, 2004.

[47] Ségolène Gauthier, André Nicolle, and Dominique Baillis. Investigation of the flame structure and nitrogen oxides formation in lean porous premixed combustion of natural gas/hydrogen blends. *International Journal of Hydrogen Energy*, 33(18):4893–4905, 2008.

[48] Ahmed F Ghoniem, Anuradha Annaswamy, Sungbae Park, and Ziaieh C Sobhani. Stability and emissions control using air injection and $h_2$ addition in premixed combustion. *Proceedings of the Combustion Institute*, 30(2):1765–1773, 2005.

[49] Bengt Lindner and Krister Sjöström. Operation of an internal combustion engine: Lean conditions with hydrogen produced in an onboard methanol reforming unit. *Fuel*, 63(11):1485–1490, 1984.

[50] John Houseman and DJ Cerini. On-board hydrogen generator for a partial hydrogen injection internal combustion engine. Technical report, SAE Technical Paper, 1974.

[51] Sebastian Verhelst and Thomas Wallner. Hydrogen-fueled internal combustion engines. *Progress in Energy and Combustion Science*, 35(6):490–527, 2009.

[52] Kap-Seung Choi, In-Jae Choi, Se-joon Hwang, Hyung-Man Kim, J Lars Dorr, and Paul A Erickson. An experimental study of methanol autothermal reformation as a method of producing hydrogen for transportation applications. *International Journal of Hydrogen Energy*, 35(12):6210–6217, 2010.

[53] Ather A Quader, John E Kirwan, and M James Grieve. Engine performance and emissions near the dilute limit with hydrogen enrichment using an on-board reforming strategy. Technical report, SAE Technical Paper, 2003.

[54] Subir Roychoudhury, Dennis Walsh, Deryn Chu, and Erik Kallio. Performance of a diesel, jp-8 reformer. Technical report, DTIC Document, 2006.